Quaternary Science Reviews 328 (2024) 108534

Contents lists available at ScienceDirect

Quaternary Science Reviews

journal homepage: www.elsevier.com/locate/quascirev

Speleothems uncover Late Holocene environmental changes across the Nuragic period in Sardinia (Italy): A possible human influence on land use during bronze to post-Iron Age cultural shifts

Andrea Columbu [a,b,*], Carlos Pérez-Mejías [c], Eleonora Regattieri [d], Federico Lugli [e,f,g], Xiyu Dong [c], Anna Depalmas [h], Rita Melis [i,j], Anna Cipriani [e,k], Hai Cheng [c], Giovanni Zanchetta [a,b], Jo De Waele [l]

[a] Department of Earth Sciences, University of Pisa, Via S. Maria 53, 56126 Pisa, Italy
[b] CIRSEC-Centre for Climatic Change Impact, University of Pisa, Via del Borghetto 80, 56124, Pisa, Italy
[c] Institute of Global Environmental Change, University of Xi'an Jiaotong, 710049 Xi'an, China
[d] IGG-CNR, Institute of Geosciences and Georesources, Via Cesare Battisti 53, 56125, Pisa, Italy
[e] Department of Chemical and Geological Sciences, University of Modena and Reggio Emilia, Via Campi 103, 41125, Modena, Italy
[f] Department of Cultural Heritage, University of Bologna, Via degli Ariani 1, 48121, Ravenna, Italy
[g] Institut für Geowissenschaften, Goethe-Universität Frankfurt, Germany
[h] Department of Humanities and Social Sciences, University of Sassari, Via Roma 151, 07100, Sassari, Italy
[i] Department of Chemical and Geological Sciences, University of Cagliari, 09042 Cittadella di Monserrato, Italy
[j] IGAG-CNR, Institute of Environmental Geology and Geoengineering, Piazzale Aldo Moro 7, 00185 Rome, Italy
[k] Lamont-Doherty Earth Observatory, Columbia University, NY, USA
[l] Department of Biological, Geological and Environmental Sciences, University of Bologna, Via Zamboni 67, 40126, Bologna, Italy

ARTICLE INFO

Handling editor: Mira Matthews

Keywords:
Holocene
Nuraghe
Nuragic culture
Bronze age
Iron age
Sardinia
Palaeoclimate
Romans
Cultural shifts
Punics

ABSTRACT

During the Bronze and Iron Age, Sardinia was home of one of the most technologically advanced Mediterranean societies (the Nuragic culture). Given its key geographical location, the island was also the fulcrum of deep cultural exchanges. Toward the end of the Iron Age, Phoenicians, and especially Carthaginians and Romans, massively frequented Sardinia for different purposes. This marks an important cultural transition for the region, as the ancient Nuragic-related society terminated. At the same time, this impacted the subsistence and land use practices. Together with middle to late Holocene climate changes, the novel anthropic activities had a pivotal role in shaping the landscape around the island. However, high resolution climate and environmental records for these culturally important phases are still lacking in Sardinia. Thus, this paper explores palaeoenvironmental changes from the Bronze Age to post Iron Ages times by using carbonate speleothems from Suttaterra de Sarpis Cave (Urzulei, central east Sardinia), strategically located nearby the Or Murales Nuragic Village. U–Th ages (n = 20) indicate that five stalagmites comprehensively span the last ~7000 years. Peculiarly, they all show an evident stratigraphic discontinuity. Age models attest that hiatuses can be at times associated with the discontinuities, spanning periods of ~1200 to ~200 years. Importantly, the discontinuities occurred from the Late Iron Age to the Roman period. Based on fabric observations, trace elements and $\delta^{13}C$- $\delta^{18}O$ analyses, the discontinuities are primarily attributed to a progressive change of land use above the cave. We suppose that deforestation aimed to clearance for agriculture and livestock practices probably was the most impacting factor for infiltration dynamics and soil state, thus affecting the studied speleothems, although archaeological and historical data are absent for the specific study area. Instead, this is in line with the cultural transition occurring in Sardinia toward the end of the Iron Age, with novel agricultural practices imported by the overseas populations. The anthropic disturbance to the millennial-long karst equilibrium possibly overprinted the response of speleothem proxies to climate oscillations, although future higher resolution analyses are necessary to better investigate the evolution of climate during the Holocene as well as its role in the development of ancient civilizations. Indeed, this is the first speleothem-based Holocene palaeoenvironmental reconstruction accomplished in Sardinia. Considering the

* Corresponding author. Department of Earth Sciences, University of Pisa, Italy.
E-mail address: andrea.columbu@unipi.it (A. Columbu).

https://doi.org/10.1016/j.quascirev.2024.108534
Received 12 December 2023; Received in revised form 30 January 2024; Accepted 30 January 2024
Available online 12 February 2024

paucity of natural lakes in this key location, speleothems here demonstrate their potential in exploring human-driven palaeoenvironmental changes during times of cultural transitions within the Mediterranean context.

1. Introduction

Sardinia, the second largest Mediterranean island, hosts one of the most important Bronze and Iron Age heritages of Italy and possibly of entire Europe (Dyson and Rowland, 2007). The most iconic artifact attributed to this period is the Nuraghe tower (1750-1150 BCE, hereafter called Nuraghe); nowadays, around 5100 of these dry-stone towers are still standing, adding to the many bedrock-carved funerary chambers, ritual/religious monolithic monuments and sacred pits encompassing the whole Bronze Age (BA) and Iron Age (IA). The function of Nuraghe is still debated, and likely changed through time (defensive and lookout, residence for important families, storage, ritual, etc.). Importantly, villages were built around many Nuraghes (Depalmas and Melis, 2011), and the activities of the inhabitants, such as agriculture, herding, timber logging, etc, developed in the surrounding areas. These activities were crucial to influence land use during the BA, IA and afterwards.

The BA-IA architectonic heritage documents the advanced technological and cultural status of Sardinia within the Mediterranean context. It is also clear that the island was a key-location for commerce. For example, goods were easily imported, while autochthonous products, especially metals, were exported around the Mediterranean and continental Europe (Eshel et al., 2019). This enduring relation with overseas populations favoured the exchange of knowledge too, in relation to arts, engineering and/or use of soil and subsistence strategies (Depalmas and Melis, 2011). For example, in the phase called "orientalising" (~700-600 BCE), as commonly reported also in other locations around the Mediterranean (Burkert, 1992), there is evidence of a change in local pottery production influenced by Levantine shapes and technology.

Notwithstanding, the IA Sardinian culture suddenly terminated at around 525 BCE because of the massive arrivals of Punic people (from Carthage, current Tunisia). Later (238 BCE), Romans took control of the island (Lilliu, 1999). Critically, the environmental scenario where this complex history evolved has never been explored in detail. More in general, Sardinia is still lacking high-resolution dated palaeoclimate and palaeoenvironmental reconstructions across BA, IA, and post-IA times. Overall, middle to late Holocene climate and environment is still poorly known. This leads to strong limitations in understanding: i) the role of climate in the development and demise of ancient Sardinian civilizations; ii) the interrelation between environmental changes, cultural exchanges, and land use. Yet, there is no chronologically constrained timeline about the use of soils during these times, as well as about the evolution of agriculture and farming practices. Indeed, the full understanding of ancient civilizations is ultimately related in comprehending the environment they lived in, and if anthropic activities had a role in shaping the landscape. Because of this incomplete background, a comprehensive picture regarding the demise of such an advanced civilisation is still missing.

The scarcity of inland palaeoenvironmental and palaeoclimate data from Sardinia can be attributed to the lack of natural lakes with extended watersheds; hence comprehensive reconstructions based on lacustrine sediments are scanty. To our knowledge, the most thorough Holocene lake-based climate reconstructions, spanning the last 8000 years, has been published only recently (Beffa et al., 2016; Pedrotta et al., 2021).

This paper aims to provide the first palaeoenvironmental reconstruction from BA to post IA times based on speleothems (cave secondary carbonate deposits). In contrast to lakes, caves abound in Sardinia as karst terrains constitute a relevant part of the territory (Carmignani et al., 2001; De Waele, 2009; D'Angeli et al., 2015). Geochemical features of speleothems such as calcite carbon ($\delta^{13}C$) and oxygen ($\delta^{18}O$) stable isotope ratios and trace elements (Mg, Sr, Ba, P, etc) give information on environmental changes occurring at the surface (McDermott, 2004; Fairchild and Treble, 2009), either naturally- (i.e. climate impact) or human- (i.e. land use impact) induced. Additionally, the fabric of calcite speleothems can deliver further evidence on the hydrological conditions during carbonate deposition (Frisia, 2015; Martín-Chivelet et al., 2017), intimately related to climate and environmental processes occurring at the surface. Considering that dating of speleothems is highly reliable (Drysdale et al., 2020; Faraji et al., 2021), these deposits have been successfully exploited to explore Holocene palaeoclimate-environment variations in different areas (e.g., Ridley et al., 2015; Voarintsoa et al., 2017; Flohr et al., 2017; Lechleitner et al., 2018; Allan et al., 2018; Baldini et al., 2019; Surić et al., 2021; Columbu et al., 2023), but, up to now, only pre Holocene records are available for Sardinia (Columbu et al., 2017, 2019).

This work focuses on five stalagmites sampled in Sarpis Cave (central east Sardinia). This cave is strategically located nearby the Or Murales Nuragic village, one of the largest ancient settlements in the Supramonte area (Lilliu, 1999). Key importance for this study is that all the selected speleothems report a marked stratigraphic discontinuity. Speleothems' fabric is here discussed, and their stratigraphy is placed into a Holocene chronological timeframe based on U–Th dating. Samples have also been analysed for $\delta^{13}C$-$\delta^{18}O$ and trace elements, to reconstruct past climate and/or anthropic driven environmental changes occurring at the study site. This paper primarily examines the environmental significance of the speleothem properties (stratigraphy, geochemical and petrographic characteristics). The aim is to disentangle the potential role of climate and/or land use changes above the studied cave, as well as to comprehend any likely interconnection between climate and anthropic factors. Along with this, we present the first Holocene speleothem-based palaeoenvironmental archive for Sardinia.

2. Area of study

Sardinia is the second largest Mediterranean island, placed in the middle of the western side of the basin. Evidences of BA-IA architecture are widespread all around the island, with ca. 5100 Nuraghes (there are possibly up to 7000, although the interpretation is controversial) and almost 300 Nuragic villages mapped so far (Fig. 1). Sarpis Cave is located in the Supramonte karst area (central eastern portion of Sardinia); it is a 200 m long single-gallery cave capped by maximum 15 m of Middle to Upper Jurassic dolostone. The latter, together with upper Jurassic calcarenites, lie unconformably on the Palaeozoic basement composed of low grade metamorphic units, quartz diorites and granodiorites (Fig. 1). For the aim of this study, it is important to highlight that Sarpis Cave is located at ca. 1 km from the Or Murales Nuragic Village (Fig. 1), originally counting at least 100 circular stone-wall structures (the base of huts) all around the main Nuraghe. The small Curcuri creek separates the village from the cave; the gently east dipping surface above the cave appears very suitable for conducting anthropic activities in the surroundings of the village (Fig. 1). Nowadays, vegetation in the study area is typical Mediterranean with bushes and widespread trees (mostly stone oaks, *Quercus ilex*). However, the Supramonte area in general is well known for olive and grapevine cultivation due to the suitable climate.

3. Materials

Five stalagmites were sampled for this study, named Sarp1 to Sarp5 (Fig. 2). Following the natural heritage conservation guidelines (Columbu et al., 2021), only broken specimens were collected. Such ethical approach implies uncertainty in reconstructing the exact location

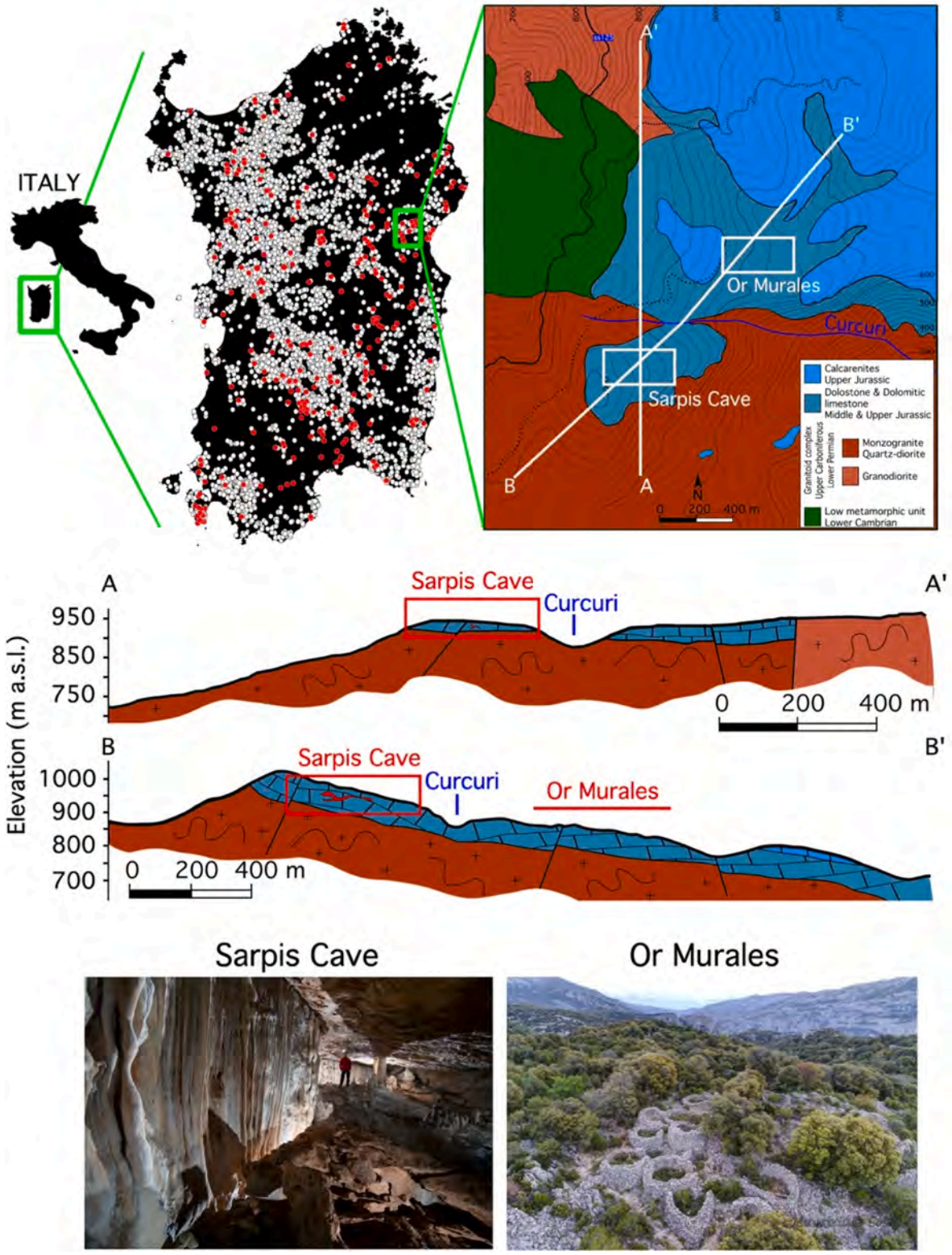

Fig. 1. Area of study. From top, map of Sardinia, reporting the Nuraghe towers (white circles) and nuragic villages (red circles), provided by the publicly available online database www.nurnet.net. The green rectangle points to the area of the Or Murales Nuragic village and Sarpis Cave, for which the geological context is provided. Sarpis Cave and Or Murales are ca. 1 km apart, separated by the small Curcuri creek. In the middle, the geological cross-sections show that the slope above the cave is minimal, and this area is easily accessible from the village, thus representing an ideal location for anthropic activities. The pictures at the bottom show the main room of Sarpis Cave (Photo V. Crobu) and the actual status of Or Murales village (Photo M. Cossu).

whence the specimens come from. All speleothems are composed of calcite (see results). Sample length is moderate: 160, 85, 150, 120, and 190 mm for Sarp1 to 5 respectively. Diameters vary from a minimum of 70 mm in Sarp2 to a maximum of 100 mm in Sarp5. Layering is visible, at naked eye, in all speleothems (Fig. 2). The most striking peculiarity characterising all samples is an evident macro discontinuity that is at 94.5 mm from the top in Sarp1, 49.5 mm in Sarp2, 65.5 mm in Sarp3, 79.5 mm in Sarp4 and 109.5 mm in Sarp5 (Fig. 2). At naked eye, it is evident that this discontinuity separates two different growth units. Indeed, besides the marked colour variation and calcite porosity, there is an enlargement of the stalagmites' diameter above the main discontinuity (Fig. Sup. 1). Moreover, below the discontinuity the shape of the layers is predominantly cylindrical, while it is mostly irregular, and at times flat, above the discontinuity. There are other discontinuities in each stalagmite, but they do not find clear inter-sample stratigraphic correlations. Thus, we refer to the feature describe above as the main discontinuity.

4. Methods

Greyscale images, following Vanghi et al. (2018), were applied to consistently identify the main growth patterns seen at naked-eye. This approach allows to detect more compact vs more porous calcite along the speleothems' layers vertical stacking (Faraji et al., 2022), being a useful tool to visualize stratigraphic discontinuities. In turn, differences in porosity are thought to reflect hydrogeological variations within the karst network (Frisia, 2015; Vanghi et al., 2018; Faraji et al., 2022). Greyscale values were calculated on high resolution RGB images of the speleothems' polished surface by ImageJ software, along a 1-pixel resolution line-scan. This corresponds to a resolution of 43 μm, 44 μm, 46 μm, 45 μm and 44 μm from Sarp1 to Sarp5 respectively. Each pixel value is the grey intensity of the 16-bit images, ranging from black (value 0) to white (value 255). Grey values were obtained averaging RGB intensities and then used to construct microstratigraphic logs based on light intensity, which were implemented by petrographic observations. For the latter, thin sections were prepared and examined under a Zeiss Axio-Zoom V16 operating at the Earth Sciences Department, University of Pisa. Fabrics were described according to Frisia (2015).

For U–Th dating, powdered subsamples of around ~100 mg were milled along a discrete number of speleothem laminae (Fig. 2), using a Dremel hand drill mounting a 2 mm diameter bit. A total of 20 samples were first dissolved using HNO_3 then spiked with a solution of known $^{236}U/^{233}U/^{229}Th$ ratio. U and Th compounds were precipitated using a Fe solution, then extracted separately using decontaminated resin columns and sequential washes of 6 N HCl and ultra-clean water to extract Th and U, respectively. Finally, the solution was mixed with 2% HNO_3 + 0.1% HF before analysis on a Thermo Fisher Neptune Plus MC–ICP–MS. Final ages were calculated, assuming a $^{230}Th/^{232}Th$ atomic ratio of 4.4 $\pm$ 2.2 $\times$ 10^{-6} and applying refined decay constants (Cheng et al., 2013). They are expressed in ka BP (thousand years before present, where present is 1950). The entire U–Th procedure, carried out at the Institute of Global Environmental Change, Xi'an Jiaotong University (China), strictly followed well-tested protocols (e.g. Cheng et al., 2020). For each stalagmite, a U–Th sampling strategy was set up to target the following areas: 1) top and bottom of each stalagmite, to determine the entire period of carbonate deposition; 2) layers just above and below the main

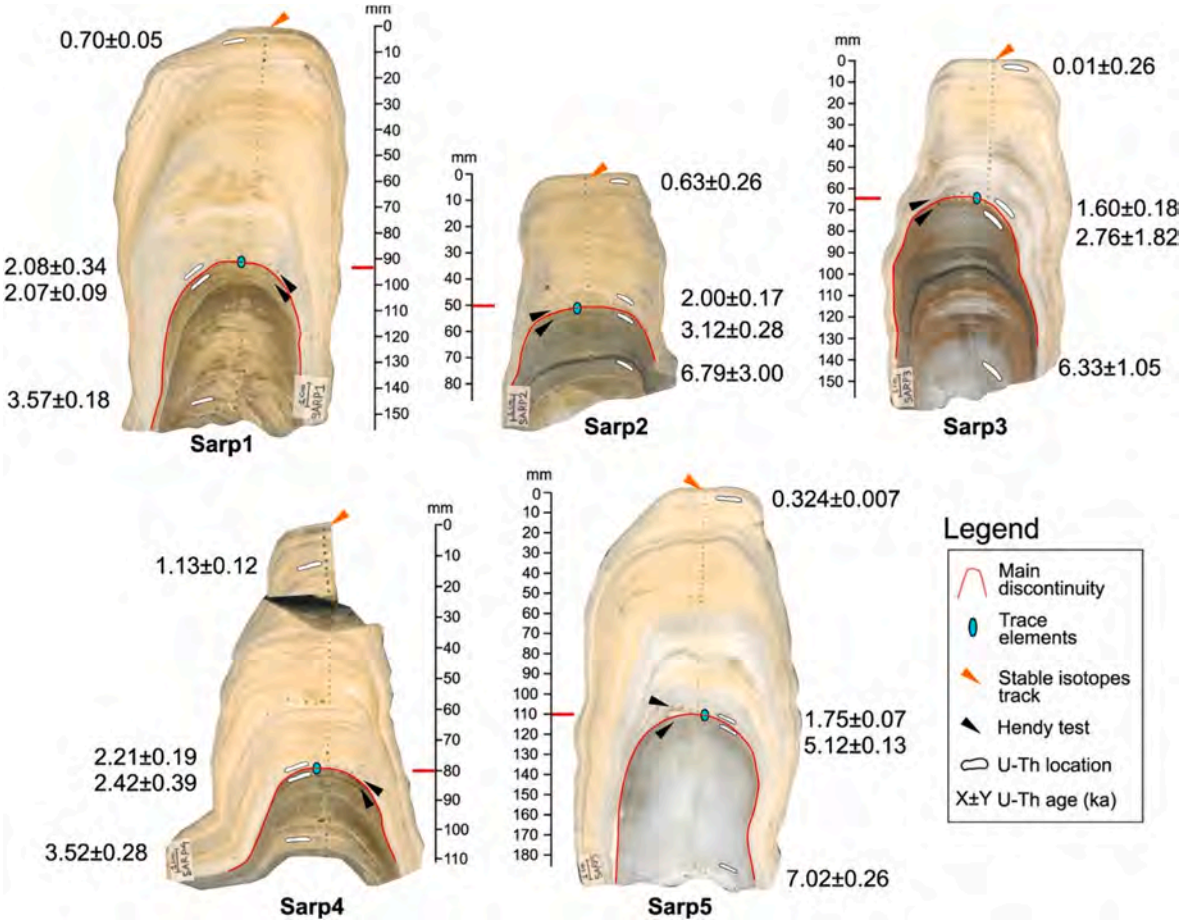

Fig. 2. Samples and analyses. The 5 stalagmites investigated in this study, reporting the subsampling location for U–Th, $\delta^{13}C$-$\delta^{18}O$ and trace elements analyses. Thin sections were instead taken from convenient locations from above, across and below the main discontinuities (see Fig. 3). The figure also reports the U–Th ages ± uncertainties (in ka).

discontinuity, in order to constrain its chronology and detect potential hiatuses. The presence of hiatuses was then tested by creating age-depth models with the COPRA algorithm (Breitenbach et al., 2012). Indeed, COPRA allows the user to manually insert hiatuses at certain depths, and running the model accordingly; this function was applied for those speleothems where, within age uncertainties, the existence of a hiatus was more likely to occur (e.g. Sarp2, Sarp3 and Sarp4). Comparison of both scenarios (non-hiatus and hiatus-bearing models) are provided when both circumstances are feasible, helping in better understanding the depositional history of the samples.

For stable isotopes ratios, ~1 mg of calcite was drilled along the speleothem axis (Fig. 2) by a Dremel hand drill mounting a 1 mm diameter bit, with a constant spacing of 3 mm. The Hendy test (Hendy, 1971) was carried out along the growth layers just below and above the detected discontinuities (Fig. 2), to discern any relevant change in depositional conditions (i.e. equilibrium vs non-equilibrium) between the two main fabrics. Analyses were done at the Institute of Earth Sciences and Georesources of the Italian National Research Council, Pisa. Briefly, powdered samples of about 0.6 mg were dissolved in H_3PO_4 (100%) and reacted at 70 °C for 1 h; the resulting gas was analysed by using a Delta Plus (Thermo Fisher) Isotope Ratio Mass Spectrometer coupled to a Gas Bench II (Thermo Fisher). Results were reported relative to the V-PDB international standard. Sample results were corrected using the international IAEA standard NBS-18 and a set of three internal standards (MOM, MS, NEW12), previously calibrated using NBS-18 and NBS-19 and by inter-laboratory comparisons. Analytical uncertainties

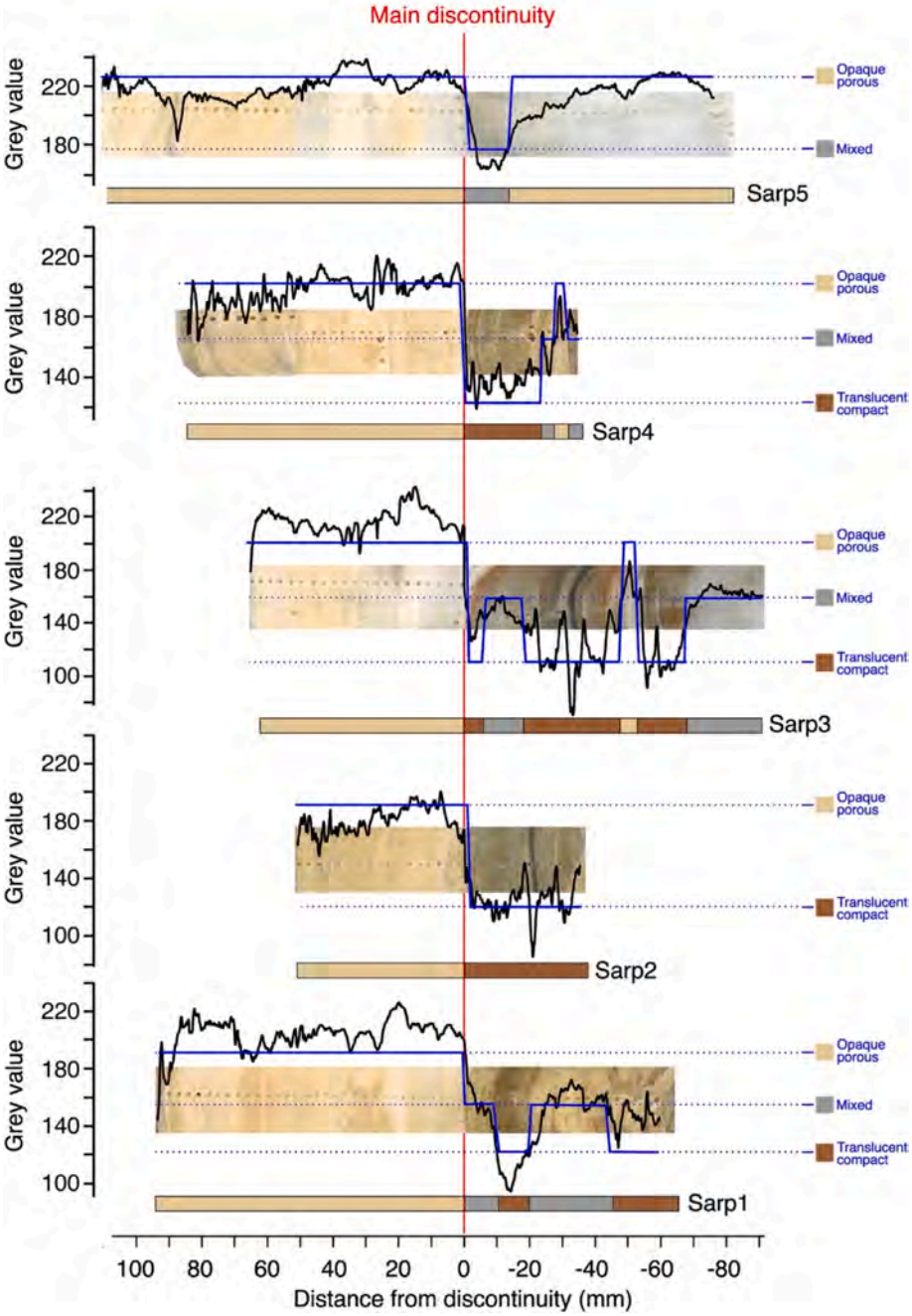

Fig. 3. Greyscale analyses. Variation of grey values (left axis and black curves) on Sarp samples. The blue curve highlights the principal fabrics (on the right, opaque porous, mixed and translucent compact) given by the greyscale. The same are identified with a coloured bar (on the bottom of each sample). The x-axis is reported as distance from the main discontinuity (red vertical line), with negative and positive depths indicating portions below and above the discontinuity respectively.

are 0.10‰ and 0.12‰ for $\delta^{13}C$ and $\delta^{18}O$, respectively.

Trace elements were measured 15 mm above and below the main discontinuities, in order to represent the major shift in precipitation environmental parameters across the main discontinuity. Analyses were performed by LA-ICP MS, using a 213 nm Nd:YAG laser ablation system (New Wave Research Inc.) coupled to an iCAP TQ ICP MS (Thermo Scientific) housed at the Centro Interdipartimentale Grandi Strumenti (CIGS) of the University of Modena and Reggio Emilia (Gatti et al., 2022; Cipriani et al., 2023). Elemental data were acquired through linear scans (i.e. one line scan per sample) along the regions of interest by using a spot-size of 55 μm, a scan speed of 15 μm/s, a repetition rate of 10 Hz and an energy density of ~5 J/cm^2. Helium (0.6 L/min) was used as carrier gas. To avoid external contamination, the sample surface was carefully pre-ablated before the actual analyses. The following isotopes (m/z) were collected: ^{7}Li, ^{23}Na, ^{24}Mg, ^{29}Si, ^{31}P, ^{44}Ca, ^{48}Ti, ^{55}Mn, ^{57}Fe, ^{63}Cu, ^{66}Zn, ^{85}Rb, ^{88}Sr, ^{89}Y, ^{138}Ba, ^{208}Pb and ^{238}U, for a total sweep time of ~0.4 s. The system was tuned for maximum sensitivity, while keeping low-oxide levels in the plasma (ThO/Th < 1%). Data were calibrated with an in-house R script by using NIST612 glass as external reference material and Ca as internal standard; in addition, the nano-powder pressed pellets NFHS-2-NP and JCt-1 were measured as quality control reference material (Weber et al., 2018; Boer et al., 2022).

5. Results

5.1. Fabric

The stratigraphic analyses detected three predominant fabrics (Faraji et al., 2022) (Fig. 3): 1) translucent compact, when greyscale values are below 150, and calcite optically appears darker under natural lights; 2) opaque porous, when greyscale values are above 180, and calcite optically appears lighter under natural lights; 3) mixed, when greyscale values range between 150 and 180, for those sections that are neither purely compact nor purely porous. The greyscale clearly identifies the main growth units seen at naked-eye. Below the main discontinuity, Sarp1 to 4 are composed of translucent compact and mixed calcite fabrics (Fig. 3). Sarp1, 3 and 4 denote an alternation of these two, with Sarp3 and 4 also having a ca. 10 mm short section, around 115 and 110 mm from the top respectively, made of opaque porous fabric. Sarp2, below the discontinuity, is entirely composed of translucent compact calcite. Sarp5 instead, below the discontinuity, shows opaque porous and mixed fabric. The latter takes place within the first 17 mm below the discontinuity. Above the discontinuity, all samples are composed of opaque porous calcite. Thus, the main discontinuity is here defined for all samples by the sharp shift toward opaque porous calcite (Fig. 3).

Microscopically, elongated columnar calcite (Frisia, 2015) dominates the portion of the stalagmites below the discontinuity (Fig. 4). Some portions of Sarp1, 2 and 4 also show fascicular optic columnar calcite. Instead, microcrystalline columnar calcite is prevalent in all stalagmites above the discontinuity (Fig. 4). Sarp4 also shows dendritic calcite. It is possible to note that the main discontinuity invariably separates columnar elongated and columnar microcrystalline calcite (Figs. 4 and 5). Additionally, in Sarp2 there are evidences of diagenesis just above the discontinuity.

According to Frisia (2015), the microcrystalline columnar and dendritic calcite types are characterised by high intracrystalline and intercrystalline porosity respectively, as well as by the presence of layers of impurities, resulting in “opaque and milky” appearance in the hand specimen. Instead, elongated and fascicular optic columnar types possess a more compact assemblage often resulting in translucent appearance. It is evident that Sarp samples agree with these features (Figs. 3–5).

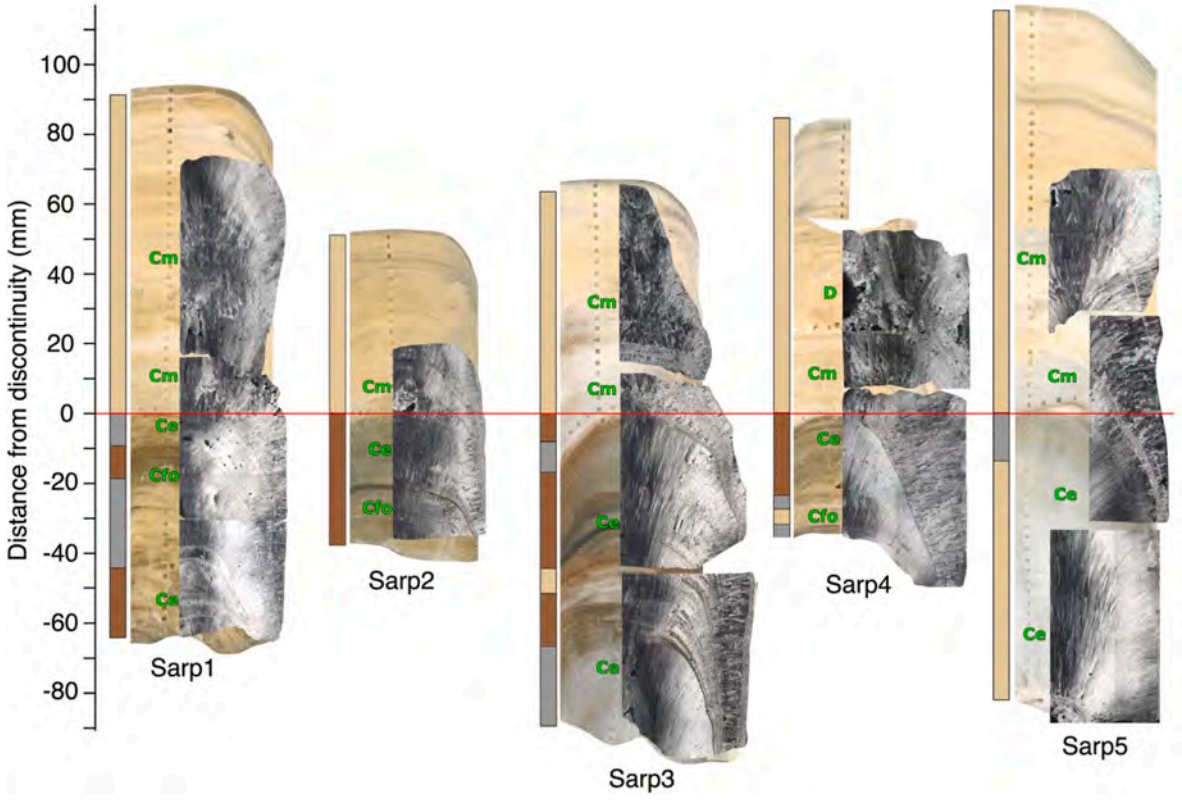

Fig. 4. Sarp thin sections. Ce, Cfo, Cm and D stand for elongated columnar, fascicular optic columnar, microcrystalline columnar and dendritic calcite. Thin section figures are taken at crossed nicols. Coloured bars are the same as Fig. 3. Stalagmite depths are reported as distances from the main discontinuity (horizontal red line), as in Fig. 3.

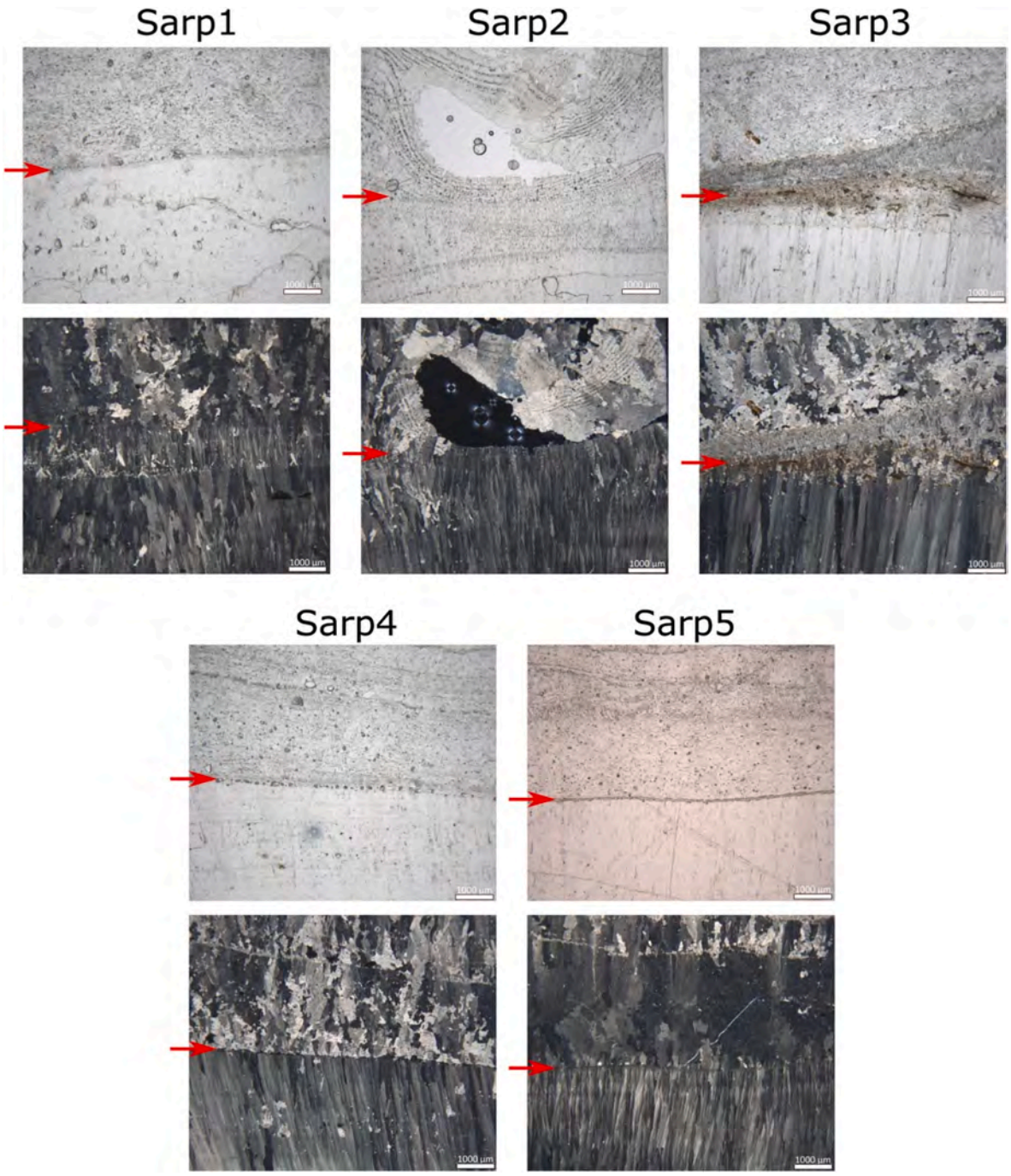

Fig. 5. Thin sections around the main discontinuities. For each sample, there is an image at parallel (above) and crossed (below) nicols around the main discontinuity. The latter is indicated by a red arrow.

5.2. Chronology

Samples selected for U–Th dating demonstrated an overall good propensity in producing reliable and accurate dates (Table 1). This is likely due to an adequate content of uranium within all speleothems (min: 36.3 ppb, max: 486.2 ppb; average: 170.6 ppb). All ages in each sample resulted stratigraphically aligned, suggesting that post-depositional effects that could potentially alter the U–Th ratios generating outliers (Bajo et al., 2016) did not occur at the selected U–Th locations. On the other hand, as common in late Holocene speleothems (Hua et al., 2012), 2σ uncertainties are at times relatively high, reflecting the low production of ^{230}Th. Even more influent on the final uncertainties is the detrital thorium (^{232}Th) contamination, expressed by the ^{230}Th/^{232}Th ratio (Table 1). Indeed, lower ^{230}Th/^{232}Th values, representing higher contamination, are generally associated to the highest uncertainties in the final ages. Sarp3-4 date, resulting in 0.015 ± 0.265 ka (Table 1), is an example of these issues. However, if excluding Sarp3-4 age (2σ >1700%), the average relative 2σ uncertainty is ~15%, with a maximum of ~65% (Sarp3-2) and a minimum of ~2% (Sarp5-7). Six out of twenty total ages show uncertainties ≤5%, while other six fall between 5% and 10%.

According to the COPRA age model, Sarp1 was deposited from $3.69^{+0.39}/_{-0.40}$ to $0.63^{+0.11}/_{-0.13}$ ka (Fig. 6). In this case the algorithm could not model any hiatus around the discontinuity; the latter is thus constrained at $2.06^{+0.18}/_{-0.17}$ ka. Sarp2, Sarp3 and Sarp4 growth patterns were instead modelled with and without hiatuses. Sarp2 grew from

Table 1
U–Th dataset.

Stalagmite	Sample ID	^{238}U (ppb)		^{232}Th (ppt)		$^{230}Th/^{232}Th$ (atomic x10^{-6})		$\delta^{234}U^{*}$ (measured)		$^{230}Th/^{238}U$ (activity)		^{230}Th Age (yr) (uncorrected)		^{230}Th Age (yr) (corrected)		$\delta^{234}U_{initial}^{**}$ (corrected)		^{230}Th Age (ka BP)*** (corrected)	
SARP1	SARP1-1	145.8	±0.5	1404	±28	69	±2	151.3	±4.9	0.0403	±0.0006	3884	±62	3640	±183	153	±5	**3.571**	**±0.183**
SARP1	SARP1_3	298.0	±1.9	1124	±32	84.0	±2.0	273.2	±4.3	0.0261	±0.00050	2257	±54	2140	±98	275.0	±16.0	**2.071**	**±0.098**
SARP1	SARP1-4	486.2	±2.1	11055	±226	24	±1	364.4	±4.4	0.0327	±0.0003	2639	±28	2154	±344	367	±4	**2.085**	**±0.344**
SARP1	SARP1-6	174.7	±0.9	490	±10	56	±2	249.5	±15.9	0.0096	±0.0003	841	±28	776	±54	250	±16	**0.707**	**±0.054**
SARP2	SARP2-1	94.8	±0.5	15392	±317	11	±0	134.9	±6.3	0.1100	±0.0020	11095	±225	6865	±3003	138	±7	**6.796**	**±3.003**
SARP2	SARP2_3	112.1	±0.5	1626	±46	40	±1	85.4	±4.4	0.0351	±0.0005	3584	±56	3195	±281	86	±4	**3.126**	**±0.281**
SARP2	SARP2-4	128.8	±0.5	1197	±25	41	±1	100.9	±4.2	0.0232	±0.0004	2324	±43	2078	±179	101	±4	**2.009**	**±0.179**
SARP2	SARP2-5	180.7	±1.3	2788	±60	13	±0	188.2	±8.0	0.0117	±0.0003	1082	±30	704	±269	189	±8	**0.635**	**±0.269**
SARP3	SARP3-1	36.3	±0.1	2704	±55	23	±1	483.9	±5.9	0.1041	±0.0026	7899	±209	6436	±1055	493	±6	**6.367**	**±1.055**
SARP3	SARP3_2	116.8	±0.3	14882	±301	9	±0	455.2	±4.6	0.0705	±0.0013	5401	±106	2833	±1822	459	±5	**2.764**	**±1.822**
SARP3	SARP3-3	106.0	±0.5	1232	±26	33	±1	337.7	±5.6	0.0235	±0.0004	1928	±35	1675	±182	339	±6	**1.606**	**±0.182**
SARP3	SARP3-4	198.0	±1.4	3304	±246	5	±0	308.7	±7.8	0.0055	±0.0003	456	±24	84	±265	309	±8	**0.015**	**±0.265**
SARP4	SARP4-1	99.7	±0.7	1450	±31	45	±1	105.4	±14.1	0.0396	±0.0008	3977	±96	3594	±286	106	±14	**3.525**	**±0.286**
SARP4	SARP4_3	113.6	±0.4	2506	±63	24	±1	168.6	±4.1	0.0322	±0.0006	3041	±56	2491	±393	170	±4	**2.422**	**±0.393**
SARP4	SARP4-4	224.3	±0.9	2673	±55	39	±1	255.2	±4.8	0.0283	±0.0003	2482	±31	2205	±198	257	±5	**2.136**	**±0.198**
SARP4	SARP4-6	109.7	±0.5	754	±15	41	±1	178.3	±5.4	0.0170	±0.0005	1584	±45	1414	±128	179	±5	**1.345**	**±0.128**
SARP5	SARP5_1	64.6	±0.2	232	±5	412	±17	408.4	±4.9	0.0898	±0.0031	7166	±257	7092	±262	417	±5	**7.023**	**±0.262**
SARP5	SARP5_4	76.1	±0.2	204	±4	401	±13	386.3	±3.3	0.0653	±0.0016	5249	±130	5193	±136	392	±3	**5.124**	**±0.136**
SARP5	SARP5-5	281.1	±2.3	1081	±24	94	±2	252.4	±15.7	0.0218	±0.0003	1916	±39	1827	±74	254	±16	**1.758**	**±0.074**
SARP5	SARP5-7	363.7	±0.9	128	±3	208	±5	208.9	±2.0	0.0044	±0.0000	402	±4	393	±7	209	±2	**0.324**	**±0.007**

U decay constants: $l_{238} = 1.55125x10^{-10}$ (Jaffey et al., 1971) and $l_{234} = 2.82206x10^{-6}$ (Cheng et al., 2013). Th decay constant: $l_{230} = 9.1705x10^{-6}$ (Cheng et al., 2013). *$d^{234}U = ([^{234}U/^{238}U]_{activity} - 1)x1000$. **$d^{234}U_{initial}$ was calculated based on ^{230}Th age (T), i.e., $d^{234}U_{initial} = d^{234}U_{measured} \times e^{l234xT}$. Corrected ^{230}Th ages assume the initial $^{230}Th/^{232}Th$ atomic ratio of 4.4 ± 2.2 x10^{-6}. Those are the values for a material at secular equilibrium, with the bulk earth $^{232}Th/^{238}U$ value of 3.8. The errors are arbitrarily assumed to be 50%. ***B.P. stands for "Before Present" where the "Present" is defined as the year 1950 A.D.

$11.55^{+9.92}/_{-7.03}$ to $0.43^{+0.53}/_{-0.55}$ ka in the case of no growth interruption and from $9.37^{+7.87}/_{-5.77}$ to $0.54^{+0.55}/_{-0.59}$ ka if a hiatus is taken into account at around the fabric discontinuity (Fig. 6). The latter is thus attested at $2.67^{+0.37}/_{-0.38}$ ka if carbonate deposited continuously, while the potential hiatus would have occurred from $2.90^{+0.62}/_{-0.65}$ to $2.25^{+0.42}/_{-0.40}$ ka. Note that the propagation of age model uncertainties at Sarp2 bottom resulted in considerably high values because of the distance from the location of the bottom date and the bottom of the stalagmite itself. Sarp3 was deposited from $8.07^{+3.16}/_{-3.04}$ to $0.01^{+0.53}/_{-0.55}$ ka in the case of no growth interruption, and from $7.22^{+2.35}/_{-2.32}$ to $0.01^{+0.56}/_{-0.53}$ ka if the hiatus actually occurred at around the discontinuity (Fig. 6). The latter is thus attested at $1.69^{+0.38}/_{-0.36}$ ka with no interruption, while the potential hiatus would have occurred from around $2.44^{+3.29}/_{-3.43}$ to $1.66^{+0.37}/_{-0.37}$ ka. Sarp4 grew from $3.38^{+0.69}/_{-0.71}$ to $1.13^{+0.34}/_{-0.39}$ ka in the case of no growth interruption and from $3.68^{+0.62}/_{-0.60}$ to $1.12^{+0.30}/_{-0.30}$ ka if a hiatus is taken into account at around the discontinuity (Fig. 6). The latter is thus attested at $2.23^{+0.34}/_{-0.33}$ ka if carbonate deposited continuously, while the potential hiatus would be from $2.41^{+0.72}/_{-0.78}$ to $2.14^{+0.39}/_{-0.38}$ ka. Finally, Sarp5 was deposited from $7.10^{+0.54}/_{-0.54}$ to $0.29^{+0.01}/_{-0.01}$ ka (Fig. 4); in this case a growth interruption is evident at around the discontinuity, and constrained from $5.09^{+0.26}/_{-0.28}$ to $1.77^{+0.14}/_{-0.13}$ ka.

5.3. Stable isotopes

Considering all five stalagmites (Fig. 7), $\delta^{13}C$ oscillates between max −4.48‰ (Sarp5) and min −11.93‰ (Sarp1); average values are instead −10.39‰ (Sarp1), −7.64‰ (Sarp2), −8.49‰ (Sarp3), −9.35‰ (Sarp4) and −9.35‰ (Sarp5). $\delta^{18}O$ reaches its maximum at −3.46‰ (Sarp1) and minimum at −6.83‰ (Sarp3), while average values are −5.25‰ (Sarp1), −4.94‰ (Sarp2), −5.46‰ (Sarp3), −5.09‰ (Sarp4) and −5.34‰ (Sarp5). Along the growth axis, $\delta^{13}C$ and $\delta^{18}O$ show a strong negative correlation (nomenclature by Cohen et al., 2013) only in Sarp5 ($r = -0.79$, $p < 0.01$), while in the other cases r-values range between −0.15 (Sarp3) and 0.39 (Sarp4).

If considering the isotopic signature of the different fabric separately, there is a strong $\delta^{13}C$-$\delta^{18}O$ positive correlation in the opaque porous calcite in Sarp1 ($r = 0.70$, $p < 0.01$), Sarp3 ($r = 0.71$, $p < 0.01$) and Sarp4 ($r = 0.74$, $p < 0.01$), placed above the discontinuity. Fabrics below the discontinuity never shows such strong positive correlation. Sarp5 differs as the opaque porous fabric predominates the whole sample and is found above and below the discontinuity; in this case, this fabric presents a strong negative correlation ($r = -0.86$) (Fig. 7a).

All $\delta^{13}C$-$\delta^{18}O$ data forms two distinctive clusters of isotopic composition by considering data from below and above the discontinuities (Fig. 7b). This is given by the general $\delta^{13}C$-$\delta^{18}O$ trend along speleothems' growth axis, where $\delta^{18}O$ increases and $\delta^{13}C$ decreases in bottom to top direction (Fig. 8a). This feature is marked for $\delta^{18}O$ but more subtle for $\delta^{13}C$. By considering the average isotopic composition from below and above the discontinuity, the most evident $\delta^{18}O$ increase is found in all samples with the exception of Sarp4 (Fig. 8b). Sarp3, 4 and 5 instead report the largest decreases in $\delta^{13}C$ average values from below to above the discontinuity (Fig. 8b). Consequently, $\delta^{13}C$-$\delta^{18}O$ variation follows, to some extent, the greyscale (Fig. 9). This is notably appreciable in $\delta^{18}O$ in Sarp1, 2 and 3.

The Hendy test (Fig. Sup. 2, Hendy (1971)) shows that: i) $\delta^{18}O$ along a single layer increases more than 0.8‰, moving from the central axis to the lateral portions of the stalagmite, in Sarp1 and 3. This occurs both below and above the discontinuity, although for Sarp3 the increase is only seen on the left side of the tested layers. In Sarp5 instead, the increase is only seen above the discontinuity. ii) $\delta^{13}C$ reports a remarkable increase (>‰) in the tested layer above the discontinuity in Sarp1, 2 and 4 (the latter only right side). In Sarp5, it is detected both below and above the discontinuity, but only on the right side. iii) along the tested layers, $\delta^{18}O$ and $\delta^{13}C$ are strongly positively correlated in Sarp4 ($r = 0.78$, $p < 0.01$) above the discontinuity, and Sarp5 both below and

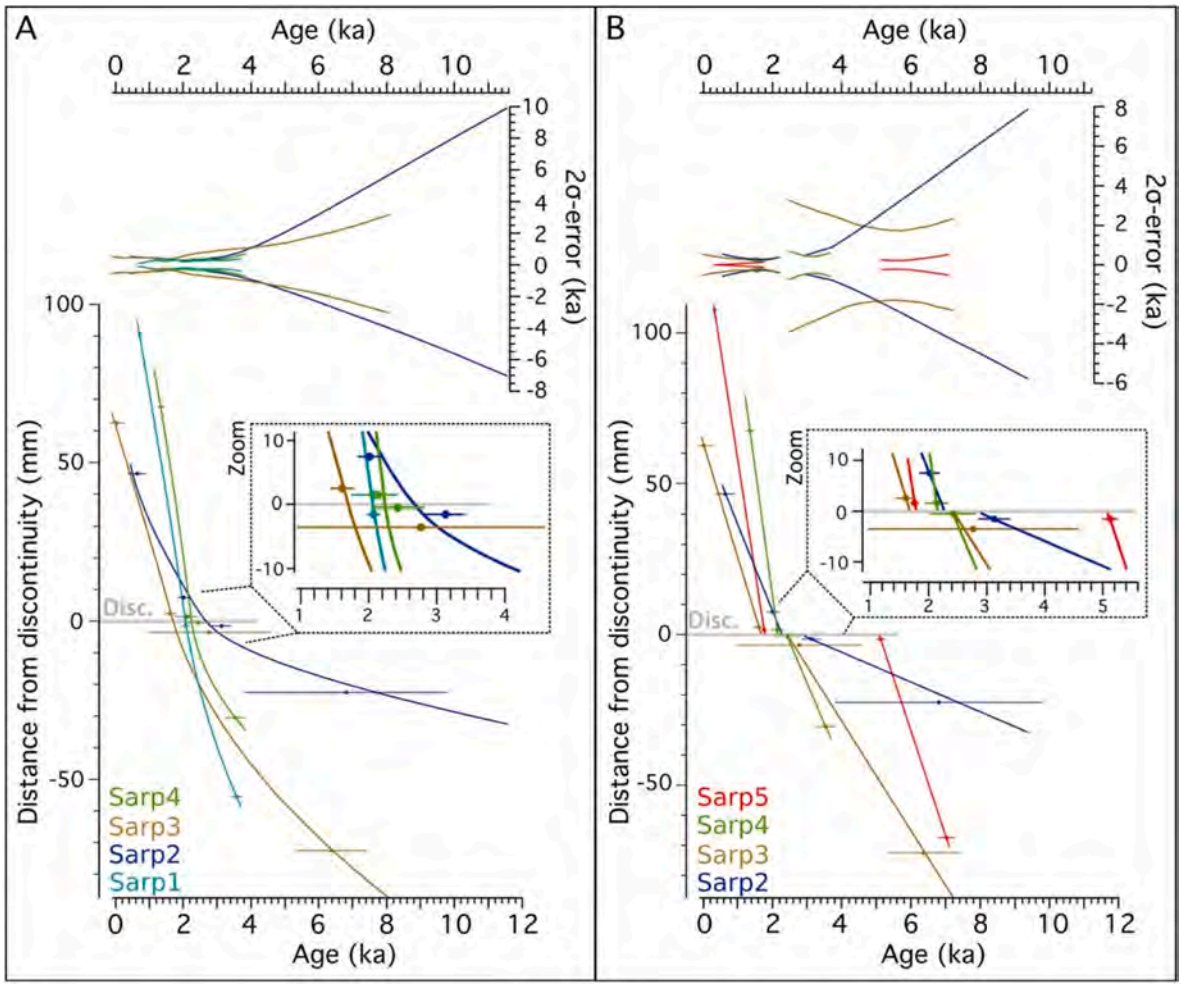

Fig. 6. Age-depth models. A) Models calculated by supposing a continuous (no hiatus) speleothem growth at the discontinuity. B) Models calculated by supposing a hiatus in the speleothem at the discontinuity. The discontinuity is reported with a grey line. In A, Sarp5 is excluded from the model as U–Th dates clearly point to a depositional stop. Similarly, Sarp1 is excluded in B as U–Th dates clearly point to a continuous growth. The panels above show the 2σ uncertainty propagation for each sample.

above the discontinuity ($r = 0.86$ and $r = 0.88$ respectively, $p < 0.01$ for both). Non-equilibrium carbonate deposition prevails if $\delta^{13}C$-$\delta^{18}O$ strongly correlate along the stalagmite growth axis and are strongly positively correlate in the tested layer, as well as if $\delta^{13}C$-$\delta^{18}O$ increase from the centre to the side of the tested layer, with a maximum increase threshold of 0.8‰ for $\delta^{18}O$. Sarp stalagmites never fulfil all these requirements (Fig. Sup. 2). However, two out of three non-equilibrium parameters are detected in Sarp1, 3, 4 and 5 but only in the tested layer above the discontinuity. Importantly, conditions of $CaCO_3$ deposition in speleothems is debated, and non-equilibrium conditions might be more common in continental carbonate than previously thought (Daeron et al., 2019). For these reasons, strong disequilibrium is certainly excluded here, but we suspect deviation from equilibrium conditions during the deposition of opaque porous fabric above the discontinuity in Sarp1, 3, 4 and 5.

5.4. Trace elements

The behaviour of the analysed elements differs in terms of concentrations and trends. Si and Mg are the only elements reaching concentrations above 1000 ppm, with the latter up to 10000 ppm in some sectors of Sarp2, 3, 4 and 5 (Fig. 10). Furthermore, Na, Fe, Ti and P vary in the range between 100 and 500 ppm, while Sr and Zn peak between 10 and 60 ppm. Ba is normally around 5–20 ppm, although showing sudden increases up to even 500 ppm (especially in Sarp1). Finally, Cu, Mn and Pb mostly oscillate between 1 and 10 ppm. Y, Li, Rb and U report the lowest concentrations (usually below 1 ppm) (Fig. 10 and Sup. 3). Of particular importance for the aim of this paper are the following features:

- P has a tendency toward higher values from below to above the discontinuity in all samples;
- Mg has a tendency toward lower values from below to above the discontinuity in all samples but Sarp1;
- Sr does not show a consistent trend considering the five speleothems;
- Si has a tendency toward lower values only in Sarp1 and 4
- Y and Zn pulse toward higher values around or above the discontinuity in all samples;
- There is a net increase of inter-element correlation (from $r > 0.3$) from below to above the discontinuity (Fig. 11), especially in Sarp3 and 4; this is evident for all elements except for Na, Ti, Sr, Ba and U.
- Sr and Mg are never correlated (with the exception of Sarp3 and Sarp2 below and above the discontinuity respectively) and Sr is the only element that below the discontinuity is correlated with more elements than above the discontinuity (Fig. 11).

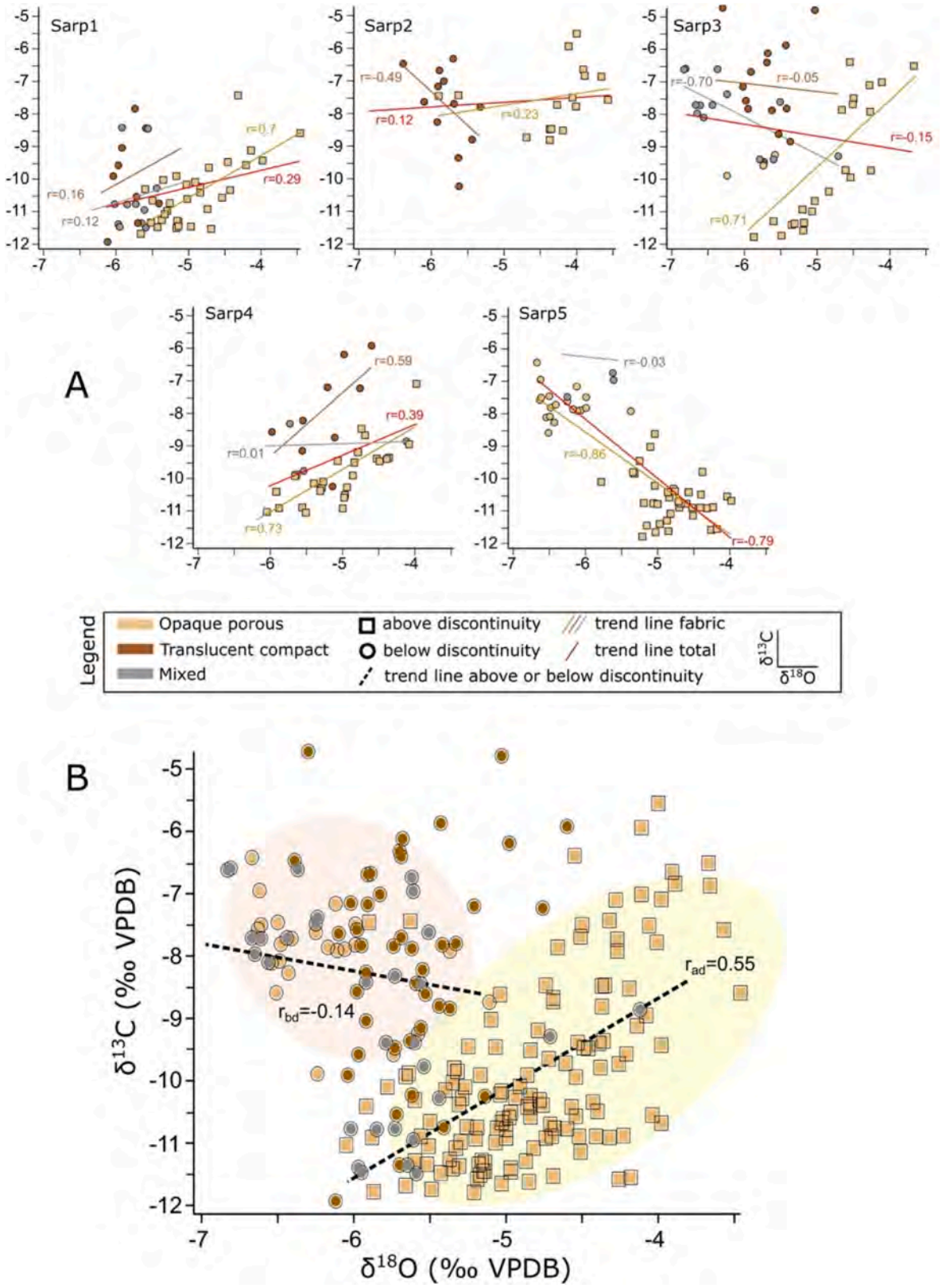

Fig. 7. $\delta^{13}C$-$\delta^{18}O$ relation in Sarp stalagmites. A) Single stalagmites $\delta^{13}C$ and $\delta^{18}O$, in y and x axis respectively. Data are reported for subsamples from below (circle) and above (rectangle) the main discontinuity. Fabric colour code refers to Fig. 3, as the trend-lines and r-correlation. The red trend line refers to the whole stalagmite. B) $\delta^{13}C$-$\delta^{18}O$ from all Sarp stalagmites, with the same symbols as A. Here, dotted trend lines refer to the portions of the stalagmites above and below the discontinuity, and relative r-values are reported as r_{ad} and r_{bd} respectively. The background shadows point to $\delta^{13}C$-$\delta^{18}O$ clusters corresponding to data above (yellowish shadow) and below (pinkish shadows) the discontinuity.

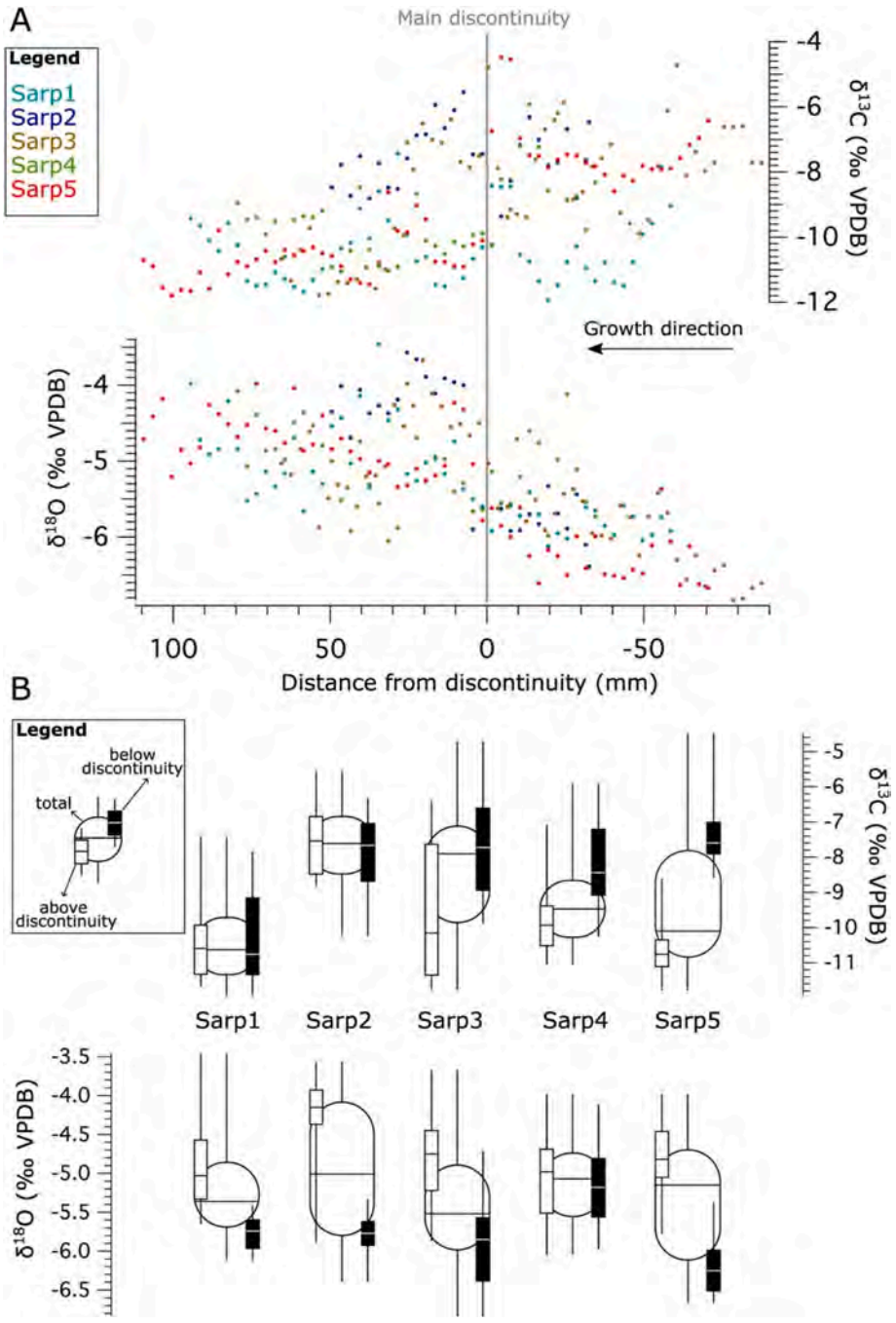

Fig. 8. Sarp $\delta^{13}C$-$\delta^{18}O$ along the axis. A) Sarp1 to 5 (see legend) $\delta^{13}C$ and $\delta^{18}O$ plotted against distances from the main discontinuity (marked as grey vertical line). B) Box and whisker plots differentiating data from below (black rectangle), above (white rectangle) the discontinuity, as the whole stalagmite (white central circle).

6. Discussion

6.1. Stratigraphic framework of the detected discontinuities

Growth units as those detected in Sarp samples are related to the environmental conditions prevailing during their deposition, in the mid- to long-term range (Martín-Chivelet et al., 2017). It follows that "*changes from one unit to the overlying one commonly represent a major shift in genetic conditions*" (Martín-Chivelet et al., 2017). In this view, and considering the chronological support (Fig. 12), translucent compact to opaque porous calcite fabrics are each testifying phases of different environmental-driven genetic conditions. Hydrological and/or geochemical variations within the seepage water may be responsible for a change in the fabric of the resulting speleothem calcite and/or layer morphology, thus procuring stratigraphic discontinuities (Frisia and Borsato, 2010). It follows that discontinuities in speleothems are potential indicators of climate-environmental changes occurring at the surface (Muñoz-García et al., 2016). This is even more straightforward when discontinuities are associated with chronological hiatuses. A growth interruption testifies that disturbances to the hydrological and/or geochemical characteristics of the seepage water led to the temporary lack of $CaCO_3$ deposition along the speleothem growth axis (Railsback et al., 2013). In Sarp1 to 4, the discontinuity pattern is similar, with opaque porous calcite replacing the translucent compact or mixed one. Microcrystalline columnar calcite type is ubiquitously present above the discontinuity, replacing the elongated columnar type

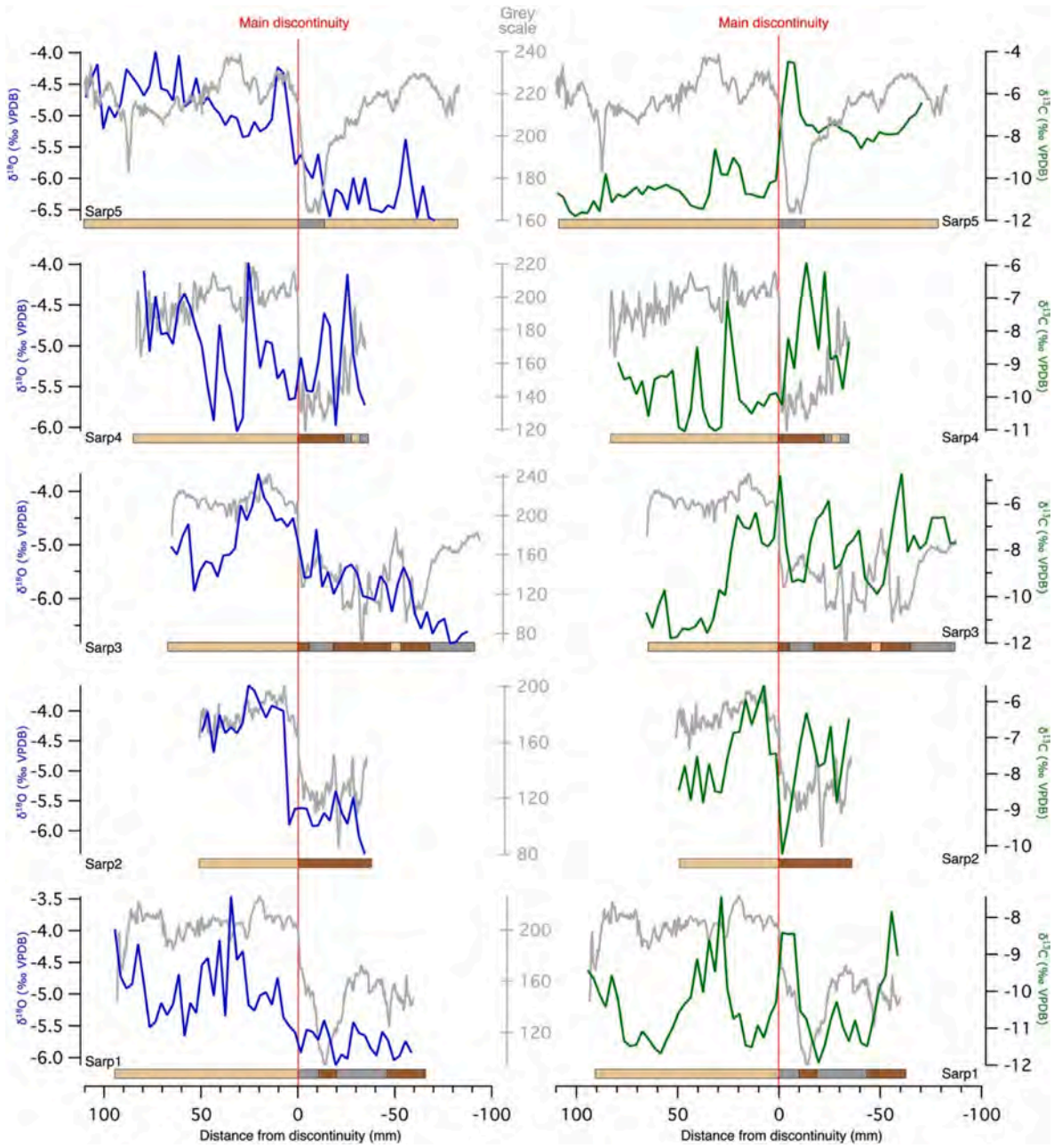

Fig. 9. $\delta^{13}C$-$\delta^{18}O$ vs greyscale. Blue and green curves are for Sarp $\delta^{18}O$ and $\delta^{13}C$ respectively. Greyscale is reported with grey curves, while the coloured bars are the same as in Fig. 3.

(Figs. 4 and 5). Indeed, it is tempting to stratigraphically correlate the four discontinuities by assuming they were generated by the same process/event. However, it is unlikely that the discontinuities were perfectly synchronous in Sarp1 to 4. U–Th dates and age modelling support that the stop of compact translucent/mixed calcite occurs instead in a period of maximum ~1200 years, from ~2.9 to ~1.7 ka (Fig. 12). The deposition of opaque porous calcite starts within a maximum of ~1000 years, between ~2.7 and 1.7 ka. These periods overlap, considering the earliest stop of translucent compact calcite deposition in Sarp2 and the latest start of opaque porous calcite deposition in Sarp3 (Fig. 12). In particular, the discontinuity in Sarp1 sharply occurred at $2.06^{+0.18}/_{-0.17}$ ka, and this is the only that is confidentially not associated with any depositional hiatus. A short hiatus might have occurred in Sarp4 (from $2.41^{+0.72}/_{-0.78}$ to $2.14^{+0.39}/_{-0.38}$ ka); if deposition here was continuous, the discontinuity would be attested at $2.23^{+0.34}/_{-0.33}$ ka. Potential hiatuses are longer in Sarp2 and Sarp3, from $2.90^{+0.62}/_{-0.65}$ to $2.25^{+0.42}/_{-0.40}$ ka, and from $2.44^{+3.29}/_{-3.43}$ to $1.66^{+0.37}/_{-0.37}$ ka respectively. If deposition was continuous, the discontinuity could have formed at $2.67^{+0.37}/_{-0.38}$ ka in Sarp2 and at $1.69^{+0.38}/_{-0.36}$ ka in Sarp3. In these cases, and possibly because of the large uncertainties, it is difficult to ascertain whether the discontinuities are synchronous with each other or not.

The characteristics of the discontinuity in Sarp5 are notably different with respect to the previous samples. Here the opaque porous calcite replaces a mixed calcite fabric that overlies a bottom sector of opaque porous fabric, with the translucent compact lacking completely. Most important, U–Th dating attests a multimillennial hiatus associated to the discontinuity, from $5.09^{+0.26}/_{-0.28}$ to $1.77^{+0.14}/_{-0.13}$ ka (Fig. 12). This signifies that the events leading to such a growth interruption are certainly much older than those related to the discontinuities detected in Sarp1 to 4. Contrarily, the recommencement of carbonate deposition in Sarp5 (i.e. $1.77^{+0.14}/_{-0.13}$ ka), characterised by the same fabric as in

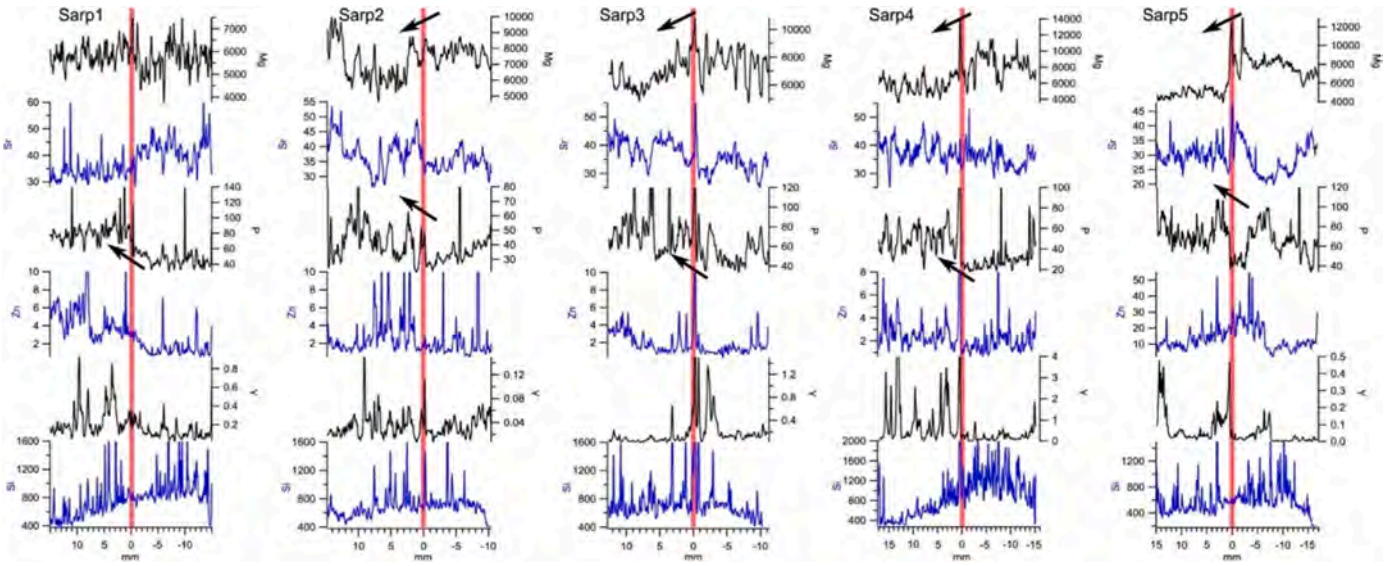

Fig. 10. Sarp trace elements. The figure reports the depth series of selected trace elements across the main discontinuity. From top to bottom of the figure, ppm variations of Mg, Sr, P, Zn, Y, and Si are reported from ca. 15 mm below the discontinuity (negative depths in x-axis) to ca. 15 mm above the discontinuity (positive depths in x-axis). The main discontinuity is indicated by a red vertical line. Arrows highlight consistent trends discussed in the text.

Sarp1 to 4, is to some extent synchronous with Sarp3 and thus chronologically close to the other samples (Fig. 12). Thus, according to the obtained chronology and fabric characteristics, discontinuities in Sarp1 to 4 are hereafter regarded as belonging to the same generation, meaning that they could potentially share the same trigger(s). At the same time, the conditions generating the restart of carbonate precipitation in Sarp1 to 4 might also be shared with Sarp5.

6.2. *Insights from fabric, $\delta^{13}C$-$\delta^{18}O$ and trace elements*

In Sarp1 to 4, the prevalent calcite type below the discontinuity (Ce, elongated columnar) is likely generated by constant drip rate, calcite saturation index (SIc) between 0.1 and 0.4 and Mg/Ca >0.3 in percolating water (Frisia, 2015). Below the discontinuity, fascicular optic columnar calcite (Cfo) is present too (Fig. 4). Cfo shares similar genetic conditions with Ce: Mg/Ca must be high ($\geq$~0.4 and $\leq$ 3), SIc at around ~0.5 and drip rate constant and/or slow or laminar flow (Frisia, 2015). Indeed, they both form from parent water where the Mg/Ca ratio is high, thus the boundary conditions determining the transition from Ce to Cfo, and *viceversa*, are at times hard to define (Frisia, 2015). Because of the high Mg environment, these fabrics usually characterise speleothems from dolostone caves. The type of calcite (Cm, microcrystalline columnar) most prevalent above the discontinuity (Fig. 4) is instead generated by water with lower Mg/Ca (<0.3) and SIc up to 0.35 (Frisia, 2015). Importantly, drip water is variable (ie. seasonal and/or flushing) and the seepage transports colloids and/or particulate. Thus, from below to above the discontinuity, the genetic environment switched to percolation favouring water with lower Mg content, and this is corroborated by the trace elements on Sarp samples (Fig. 10). The latter show a substantial decrease of Mg across the discontinuity in all samples but Sarp1.

In caves carved in dolomitic bedrock, speleothems' lower (higher) Mg content has been attributed to reduced (prolonged) water-rock interaction (Orland et al., 2014). This can be associated to wetter periods favouring shorter residence time and *viceversa*. If so, from below to above the discontinuity there would have been a shift from general drier to wetter conditions. $\delta^{13}C$ data seems to corroborate this view as the trend, although faint, toward more negative values (Figs. 8 and 9) indicates a high vegetation activity usually favoured by wetter and warmer conditions. Speleothem $\delta^{13}C$ in the Mediterranean context (Bernal-Wormull et al., 2023), and specifically in Sardinia (Columbu et al., 2017, 2019), has indeed been proven as a proxy for climate-driven soil bioactivity. However, during wetter periods the so-called amount effect would drive speleothem $\delta^{18}O$ toward more negative values (Drysdale et al., 2009), which is not occurring in Sarp samples (Figs. 8 and 9). Additionally, calcite fabrics above the discontinuity cannot sustain an increase in rainfall.

Oppositely, a marked aridification trend has been detected in the Padul Basin, southern Iberian Peninsula (Ramos-Román et al., 2018), during the last ~5000 years. A similar trend is visible in Sicily using lacustrine sediments too (Zanchetta et al., 2022). The bottom to top increasing trend of $\delta^{18}O$ in Sarp stalagmites seems in agreement. However, as southern Iberia and Sicily are way more south with respect to the Sarpis study area, it is possible that the impact of the aridification has been milder in Sardinia, as already reported for other Central and Northern Italian mainland locations (Sadori et al., 2011). This would have contributed to the multimillennial drift of Sarp $\delta^{18}O$ toward higher values because of the amount effect. The fabrics above the discontinuity are coherent with this scenario, as a general reduction of rainfall would generate variable dripping. However, $\delta^{13}C$ trend is not fully sustaining this scenario. This means that different processes other than climate possibly had a role in driving $\delta^{13}C$-$\delta^{18}O$ of speleothems in the study area.

The Holocene is also punctuated by rapid climate oscillations (Fig. 13). The most important drying episodes, chronologically closer to the studied speleothems, are the regional 4.2 event (Zanchetta et al., 2016), and a possibly more local one identified by speleothems and lake levels in the Italian mainland at 3.1 ka (Magny et al., 2007; Regattieri et al., 2014). A compilation of central Italian archives identified a climatic instability around 2 ka (Bini et al., 2020) during the so-called Roman Climatic Optimum (RCO, Harper, 2017). Indeed, a short-scale arid phase detected also by the rainfall anomaly index from Corchia Cave (Regattieri et al., 2014), started at 2.3 ka and peaked at 2.05 ka, with driest conditions lasting for maximum 30 years (Bini et al., 2020). This is followed by an abrupt transition to a wetter period lasting ca. 100 years, from ~2 to ~1.9 ka (Bini et al., 2020) (Fig. 13). Unfortunately, the chronological resolution of Sarp makes the correlation with these events difficult. However, we highlight that intense multicentennial climate pulses would have generated pulse-like Sarp $\delta^{13}C$-$\delta^{18}O$ oscillations toward the same direction, because of the concurrence of the rainfall amount effect and soil bioproductivity variations (Columbu et al., 2017, 2019). Around the discontinuity, this is only visible in Sarp2 (Fig. 9). At the same time, extreme aridity would have caused

discontinuities, and possibly hiatuses, synchronous within all speleothems. Thus, it is unlikely that the peak of arid conditions detected in Central Italy at 2.05 ka was the main cause for the genesis of the discontinuity in all Sarp samples.

The divergent behaviour of $\delta^{13}C$-$\delta^{18}O$ across the discontinuity cannot be explained by geochemical processes occurring in the epikarst (e.g. prior calcite precipitation (PCP)) or in the cave (e.g. strong disequilibrium). This is because they would have affected $\delta^{13}C$-$\delta^{18}O$ in the same direction, leading to higher values in both species (McDermott, 2004). Moreover, the Hendy test is not procuring definitive evidences for calcite deposited under disequilibrium conditions in all samples (Fig. Sup. 2), and the lack of Mg–Sr correlation (Fig. 11) points to the absence of PCP (Fairchild and Treble, 2009).

It has been recently proved that $\delta^{18}O$ in coeval speleothems from the same cave often diverges due to the influence of fractures on flowpath (Treble et al., 2022). Although this study ignores the information given by speleothem stratigraphy and fabric, it warns in attributing the meaning of $\delta^{18}O$ without considering the role of the feeding system. The latter can vary from fracture-flow, matrix-flow and multiple combinations of these two, basically impacting every single dripping $\delta^{18}O$ within the same cave. In Sarp stalagmites, the portions below the discontinuities of Sarp1 and 4 can be considered as coeval (Fig. 12); however, their average $\delta^{18}O$ differs by 0.5‰ (Fig. 8), with Sarp1 showing a lower average value as well as lower variability. According to Treble et al. (2022), the lower average value signifies that Sarp1 is fed by a degree of fracture flow that is higher than Sarp4, although the low variability is in contrast with this scenario. More in general, Treble et al. (2022) highlights that the more the speleothems are fed by a higher degree of fracture flow, the more their $\delta^{18}O$ would potentially respond in a non-linear behaviour with respect to hydroclimate forcing. This non-linearity would increase during periods of higher rainfall, when a larger contribution of fracture flow is activated. Unfortunately, the lack of monitoring data at Sarpis Cave impedes to discuss in detail the karst hydrological control on $\delta^{18}O$. However, while we acknowledge this could have had a role in modulating Sarp $\delta^{18}O$, we find it hard to attribute the consistent $\delta^{18}O$ enrichment trend in Sarp stalagmites to the ratio of fracture vs matrix flow(Fig. 8) from below to above the discontinuity, considering they are not all coeval. At the same time, if the feeding system was highly different for the five stalagmites, we would not expect such a similarity in fabric (Fig. 4), trace elements

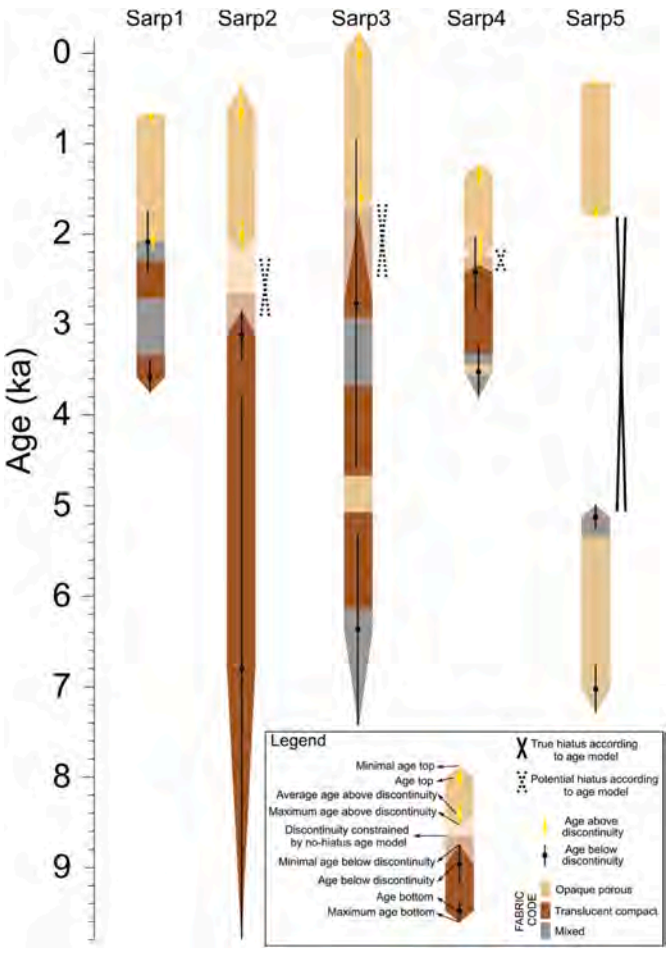

Fig. 12. Stratigraphy of Sarp stalagmites. Coloured bars are the same as Fig. 3 (see fabric code in the legend), here plotted vs time (ka) after age modelling. In Sarp2, 3 and 4, there is the possibility of either a hiatus or no hiatus associated with the main discontinuity (see text).

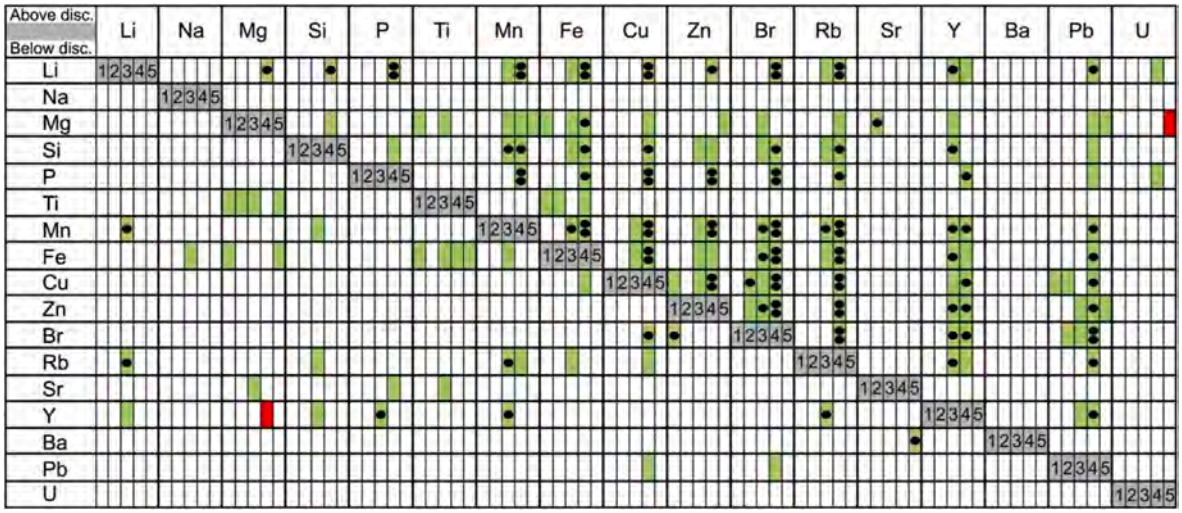

Fig. 11. Trace elements r-coefficients. The chart is divided in two parts, above and below the grey cells, corresponding to portions of the stalagmites above and below the main discontinuity respectively. The grey rectangles are numbered from 1 to 5, corresponding to Sarp samples from 1 to 5. Green cells correspond to positive r-coefficients between 0.3 and 0.39 (weak correlation); in green cells with a dot r is between 0.4 and 0.69 (modest correlation), while in green cells with two dots r is between 0.7 and 0.89 (strong correlation). Red cells indicate negative r-correlation between −0.3 and −0.39. Empty cells mean r values between −0.29 and 0.29 (very weak or no correlation). The nomenclature provided is from Cohen et al. (2013). P-value is always attested <0.001. The graph reads by intersecting elements from the vertical and horizontal axis, belonging to samples from Sarp1 to 5.

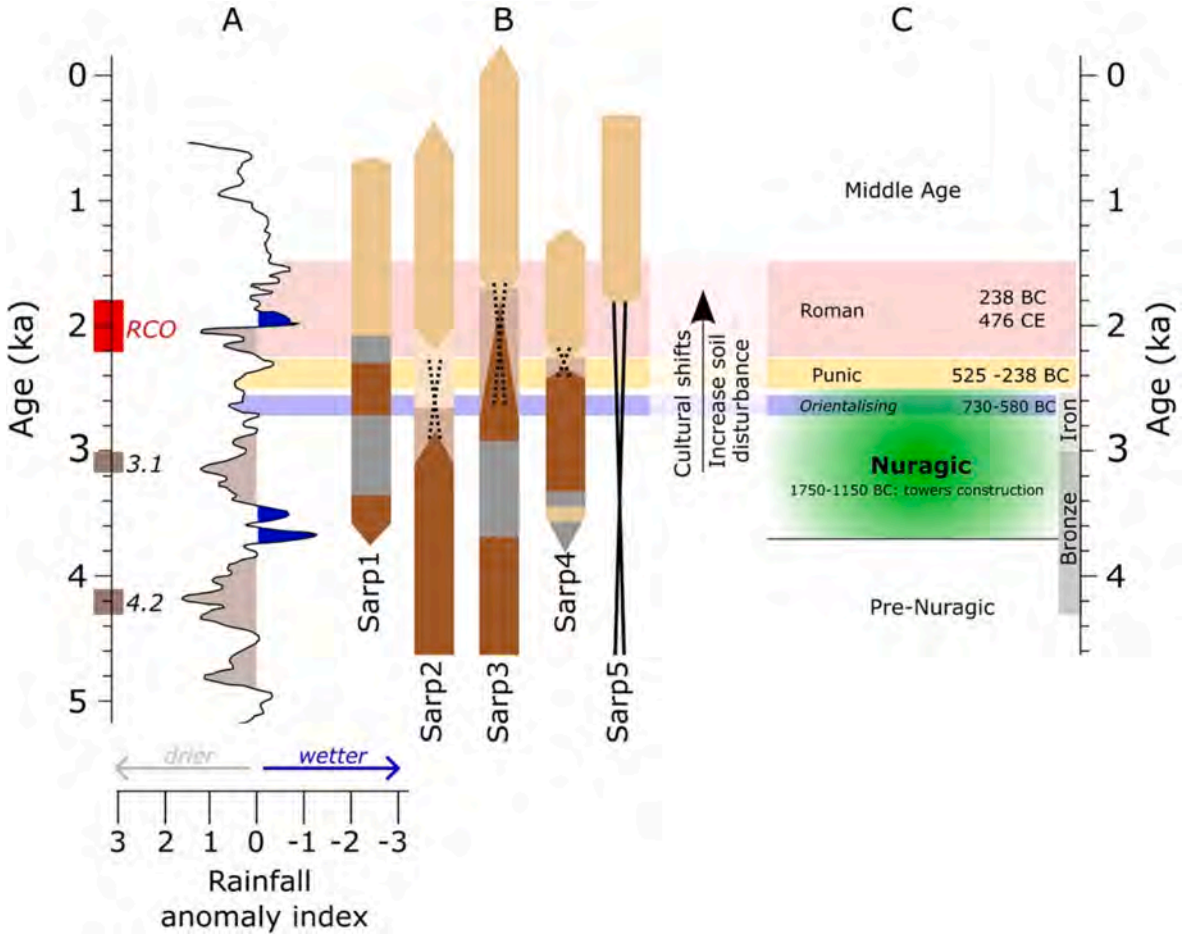

Fig. 13. SARP stratigraphy into the climate and historical context. A) Rainfall anomaly index from Corchia Cave (Central Italy, Regattieri et al., 2014), for the last 5000 years. The main wetter vs drier phases are reported with blue and grey shading respectively. Climate phases discussed in the text are reported along the left age axis, as the 4.2and 3.1 events, as well as the Roman Climate Optimum (RCO); note that the latter is composed of a drier phase followed by a wetter period (Bini et al., 2020). B) The same as Fig. 12. C) Main cultural transitions in Sardinia, with the pre-Carthaginians arrival period (green shading) characterised by the Nuragic and post-Nuragic (Sardinian Late Bronze and Iron phases) culture. The Orientalising phase took place during the Iron Age (purple shading). Carthaginians (Punic period) massive arrival in the island occurred at the very end of the Iron Age (yellow shading), while Romans took control of Sardinia afterwards (brown shading). The black arrow symbolises the increase of soil disturbance (see text) during times of important cultural shifts.

trends (Fig. 10) and correlation (Fig. 11).

Also, the Cm fabric suggests that the content of colloids increases, and the evident higher P content from below to above the discontinuity (and in less extent Zn and Y) is a further evidence (Fig. 10). This is because P is transported in colloids and, together with Y, Zn, Cu and Pb, have been related to the mobilisation of organic acids from the soils. For example, Borsato et al. (2007) used these species to detect seasonal flushes of organic matter in north-eastern Italian speleothems. Besides colloids, Cm calcite traps mineral particulate, commonly enriched in elements such as Si, Fe, Al and Mn. For instance, short-lived increases in Si in a central Italy speleothem have been linked to high infiltration rates from a catchment having a thin soil, with reduced capacity for the retention of mineral particles (Regattieri et al., 2016). In general, colloids and particulate-derived elements show higher correlation when the allochthonous fractions have the same source and/or they are mobilized contemporaneously (Regattieri et al., 2016). In Sarp stalagmites, it is evident that, above the discontinuity, elements likely deriving from mineral particles (Si, Fe and Mn) and colloids (P, Y, Zn, Cu and Pb) are positively correlated (Fig. 11). Remarkably, even Mg from below to above the discontinuity, shows a higher correlation with respect to these elements. Contrarily, only Na, Ti and-most importantly- Sr, Ba and U do not show any increase in correlation from below to above the discontinuity (Fig. 11). This clearly indicates that particulate and colloid inputs have the same behaviour in the portion of the stalagmites above the discontinuity, differently from what has been detected below the discontinuity. This somehow involves a detrital source for Mg too, and thus there is a further evidence that it cannot be taken as bedrock-leaching indicator. The outcropping Palaeozoic basement nearby the study area (Fig. 1) would offer a likely preferential source for detrital Mg. Instead, the lack of Mg correlation with elements leached from the carbonate bedrock and likely transported as solutes (Sr, Ba and U, Fairchild and Treble (2009)) means that any process triggering the outlined difference in elements correlation must have occurred at the surface, i.e. at the soil level.

6.3. Cultural shifts promoting environmental changes in Sardinia: a background for interpreting Sarp data

Geochemical data are pointing toward surface-, rather than karst-related primary influences in modifying the speleothem genetic conditions. Importantly, as the discontinuity in Sarp1 to 4 samples is not synchronous, the environmental changes occurring at the surface were gradual rather than sudden. Thus, the opposite behaviour of $\delta^{13}C$-$\delta^{18}O$ across the discontinuity, pointing toward lower and higher values respectively, might be the result of localised phenomena affecting only one isotopic species. The same were able to modify the infiltration rate inducing a shift from constant/low to variable/flushes-like drip rate in the cave, also allowing a higher availability of particulate and colloids

from below to above the discontinuity. The likely presence of colloids, corroborated by the higher concentration of P above the discontinuity, point to a constant soil activity, confirmed by the faint shift toward lower $\delta^{13}C$ values from below to above the discontinuity. Instead, the prominent drift of $\delta^{18}O$ toward higher values can be the result of reduced rainfall and/or water evaporation at the surface, with no direct effects on $\delta^{13}C$. For the reasons explained above, it is hard to sustain that the area was affected by an intense decline of rainfall. Thus, the focus here is the occurrence of localised evaporative phenomena. Importantly, evaporation at the surface would lower the precipitation/evapotranspiration ratio, decreasing the effective recharge to the karst aquifer and thus finally impacting on the dripping in the cave.

We note that the detected discontinuities in Sarp1 to 4 occurred during periods of intense cultural changes in Sardinia (Fig. 13). All around Or Murales (i.e. ca. 10 km radius) there are 10 other Nuragic villages as well as ca. 50 Nuraghes (Fig. 1), meaning that this portion of Sardinia was densely inhabited during Nuragic times. Unfortunately, there are no exhaustive archaeological and historical studies carried out at Or Murales, but we can suppose this village had a comparable evolution with respect to the cultural and social trends occurring throughout the island. Indeed, the edification of towers ceased at around ~3.1 ka (1150 BCE, late BA) (DePalmas, 2018), but the existent ones were restored or expanded, being dwelling places until Roman times or later (Delussu, 2016). By time, towns developed around the main Nuraghe, a feature still visible today insofar some modern cities in Sardinia display a Nuraghe tower within the ancient nucleus. A recent study proved that Nuragic people developed their land occupation strategies by transforming the landscape into agro-silvo-pastoral systems (Malvasi et al., 2023), producing wood grasslands structurally similar to Savannas. This involves localised clearance to allow the simultaneous activity of forest product harvesting, livestock and agriculture. Palynological findings from different areas of Sardinia support this scenario, assessing a gradual deforestation throughout the BA with no consistent changes in species (Bakels, 2002; López et al., 2005; di Rita and Melis, 2013; Buosi et al., 2015; Beffa et al., 2016; Pittau et al., 2018; Pedrotta et al., 2021). Also, during middle BA, bronze axes and pans are widespread, indicative of more deforestation (Depalmas and Melis, 2011). However, these practices were possibly limited around the dwelling places, aimed to local livestock and cultivation of cereals and legumes (Ucchesu et al., 2015). Bone remains of game are predominant, confirming that most of the territory was still covered with well-developed forests. Agriculture and grazing strongly developed from the late BA and then IA (Sabato et al., 2019). At these times, the millennial long autochthonous Sardinian culture had a peak of cultural exchanges during the orientalising phase (~2.7-2.5 ka, 730-580 BCE, Fig. 13), leading to a net change in art and costumes (Burkert, 1992). Within this phase Phoenicians, from the Levant, also established permanent coastal colonies in Sardinia, possibly because of their quest for metals and other supplies (Eshel et al., 2019). Later on, Punic people from Carthage (current Tunisia) arrived in Sardinia (~2.5 ka, 525 BCE, Fig. 13); within two centuries, there was the capillary inland penetration by Punics targeting the metallurgical districts as well as the most fertile locations. By also obtaining the political control of the island, the arrival of Punics marks the major cultural shift of these ancient times (Depalmas and Melis, 2011), testified by deep changes in the funerary customs and structures, production of pottery as well as craftsmanship in general (Bernardini, 2009). This is coincident with the end of the Sardinian IA culture. Afterwards, Rome defeated Carthage (~2.2 ka, 238 BCE, Fig. 11), and Sardinia mostly became a Roman metallurgical and agricultural colony. Importantly, Phoenicians, Carthaginians and Romans brought new practices into the island, and contributed to modify those already existing. There was the introduction of new crops (Ucchesu et al., 2017) and holm oaks replaced cork oaks at around 2.5 ka (Pedrotta et al., 2021) during the orientalising phase and Punic arrival. This is correlated to intensifying farming activities by Phoenicians, Carthaginians and later Romans and the necessity of bark and acorns, the latter used as fodder for livestock purposes (Pedrotta et al., 2021). As consequence, deforesting was also a common practice, for timber as well as obtaining open space for agriculture and farming.

All in all, it can be stated that the trend of human disturbance on the Sardinian environment started within the Nuragic culture, and intensified during the orientalising, Punic and Roman phases. Clearance had a crucial role in transforming the landscape around the Mediterranean basin, which possibly has been completely moulded by humans throughout the Holocene (Blondel, 2006). We stress that there are no specific archaeological and historical studies for Or Murales, but it is likely that the area around the village experienced the same evolution as other locations in the island following the main cultural shifts outlined above.

6.4. *Sarp speleothems possibly record human-driven environmental changes around Or Murales village*

Since cultural evolution during Nuragic and post Nuragic times involved changes on the use of soils in Sardinia, we question if human activities may have had an environmental impact in the study area, thus contributing to rule Sarp speleothems' stratigraphy, geochemical composition and petrographic characteristics. Indeed, anthropic activity can deviate the natural climate-environmental driven isotopic signal (Regattieri et al., 2019) by modifying infiltration dynamics. These latter control the resulting fabric as well as the partition of trace elements in speleothems. Considering that the area above the cave: i) is easily reachable from the Or Murales village; ii) is mostly flat; iii) water is available, at least seasonally, in the Curcuri creek (Fig. 1), it is likely that several activities involving land use were accomplished there. The activities might have induced a disturbance to the local infiltration dynamics, which possibly had previously reached a multi-millennial equilibrium status. We consider deforestation aimed to clearance for agriculture and livestock practices as the most impacting factor for infiltration dynamics, affecting the studied speleothems considering:

- the increased $\delta^{18}O$ given by enhanced evaporation at the soil surface (i.e. before infiltration);
- the slight decrease in $\delta^{13}C$ given by increased soil bioactivity because of agriculture and farming; this also increases P, especially because of farming;
- irregular cave dripping because of the absence of tree canopy and possible actions of irrigation and ploughing; in this circumstance, infiltration and biological activity is strongly seasonal, thus aquifer recharge is more subjected to flushes and the amounts of soil CO_2 are highly variable.

The latter is suspected to have multiple effects on speleothem growth, as:

- the disturbance to a multimillennial hydrological equilibrium might cause the temporaneous lack of dripping and/or supersaturation with respect to $CaCO_3$, and thus hiatuses;
- irregular dripping promotes Cm calcite, rather than Ce/Cfo;
- flushes mobilise colloids and mineral detrital particles together.

As reported above, there are no evidences on deforestation timing and dynamics for the Or Murales area, but these might have occurred in concert with the social and cultural development of the entire island. Presumably, locals started with gradual deforestation during the IA, coinciding with the discontinuity detected in Sarp2 (Fig. 13). Initially, it only involved a small fraction of the territory above the cave. Although it is difficult to sustain without any archaeological evidence, this might have occurred because of the development of the Nuragic culture and/or the new practices introduced by the orientalising phase. The clearance was thus aimed for agriculture and/or farming, at least around the Or Murales village. Through time, a progressively larger area was targeted

for deforestation, during the Punic Period (discontinuity in Sarp4) and then in Roman times (discontinuities in Sarp1 and 3). With this scenario, we can envision a strong environmental disturbance to the millennial hydrological equilibrium, interrupted by the discontinuities. At the same time, the disturbance is differential through space and time, the reason why the same generation of stratigraphic discontinuity is not occurring perfectly synchronous, as was expected if the entire area was deforested in a short time.

Finally, it is interesting to note that at around ~1.7ka, deposition of the opaque porous fabric was active in all stalagmites, including Sarp5 (Fig. 13). In the latter, the precipitation of $CaCO_3$ restarted after the detected multimillennial hiatus. We interpret this comprehensive behaviour by considering the establishment of a new full equilibrium state of the hydrogeological circulation, leading to the genesis of the opaque porous unit for many millennia ahead. It is possible that this renovated "carbonate factory" (James and Jones, 2015) was sustained by the combined effect of i) stability of anthropic activity during Roman times; and ii) the favourable climate conditions during the wetter phase within the RCO (Fig. 13) (Bini et al., 2020).

7. Conclusions

This study established that discontinuities in Sarp stalagmites, as well as major geochemical and petrographic variations, are chronologically correlated to a prolonged phase of intense cultural changes occurred, in Sardinia, since late Nuragic times. There are no archaeological and historical evidences that these changes specifically impacted the Or Murales area, but it is presumed these acted in concert with the social evolution of the island. Particularly, discontinuities start toward the end of the IA, when the commercial network is highly developed and the arrival of overseas population, at times settling permanent colonies, is massive. The evolution of the indigenous society first, coupled with new costumes introduced by Phoenicians, Carthaginians and Romans, led to new practices in the use of soils in Sardinia, and presumably around the study area. Indeed, the flat surface above the cave is here considered as ideal for sustaining practices related to the every-day life at Or Murales Nuragic village. Deforestation, as common in other portions of the island, was possibly aimed to forest clearance for agriculture and farming. This induced a disturbance into the millennial-long soil and hydrogeological natural processes that, besides the stratigraphic discontinuities themselves, imprinted the $\delta^{18}O$-$\delta^{13}C$, trace elements and fabric characteristics of the carbonate stalagmites. Thus, this study hypothesises that anthropic activities having a substantial impact onto the environment, and boosted by cultural changes into the ancient Nuragic-related Sardinian civilization, are recorded by the studied speleothems. Noteworthy, the Sarp data well-fit within the recent global synthesis of land-use for the last 10 kyrs, which reveals a planet Earth deeply transformed by growing communities of hunter-gatherers, farmers, and pastoralists by 3 ka (Stephens et al., 2019).

At the same time, we only found subtle evidences of the Holocene aridification trend over the last ~5000 years, which is instead well evident at other Mediterranean locations. This is possibly due either because the climate signal is concealed by the disturbances induced by anthropic activities and/or Sardinia was less affected by such multimillennial phase. Concurrently, the resolution of the presented analyses is possibly not sufficient to detect very rapid Holocene climate oscillations, such as the 4.2, 3.1 or the RCO events. With future higher resolution analyses, it will be possible to better explore if climate co-participated in inducing environmental and/or cultural shifts in Sardinia.

Speleothems here further demonstrate their potential in investigating human-driven palaeoenvironmental changes during times of rapid and important cultural shifts within the Mediterranean context. They thus represent a valuable tool for complementing archaeological studies.

Declaration of competing interest

The authors declare that they have no known competing financial interests or personal relationships that could have appeared to influence the work reported in this paper.

Data availability

Data will be made available on request.

Acknowledgments

We are grateful to local speleologists that helped us during cave sampling, and to Prof. Bersani D. (Parma University, Italy) for attempting preliminary analyses. We also thank the Urzulei municipality for permitting this study. Finally, the comments of Dr. Gabriella Koltai and three anonymous reviewers substantially improved the quality of the manuscript.

Appendix A. Supplementary data

Supplementary data to this article can be found online at https://doi.org/10.1016/j.quascirev.2024.108534.

References

Allan, M., Deliège, A., Verheyden, S., Nicolay, S., Quinif, Y., Fagel, N., 2018. Evidence for solar influence in a Holocene speleothem record (Père Noël cave, SE Belgium). Quat. Sci. Rev. 192, 249–262.

Bajo, P., Hellstrom, J., Frisia, S., Drysdale, R., Black, J., Woodhead, J., Borsato, A., Zanchetta, G., Wallace, M.W., Regattieri, E., 2016. "Cryptic" diagenesis and its implications for speleothem geochronologies. Quat. Sci. Rev. 148, 17–28.

Bakels, C., 2002. Plant remains from Sardinia, Italy with notes on barley and grape. Veg. Hist. Archaeobotany 11 (1), 3–8.

Baldini, L.M., Baldini, J.U., McDermott, F., Arias, P., Cueto, M., Fairchild, I.J., Hoffmann, D.L., Mattey, D.P., Müller, W., Nita, D.C., 2019. North Iberian temperature and rainfall seasonality over the younger dryas and Holocene. Quat. Sci. Rev. 226, 105998.

Beffa, G., Pedrotta, T., Colombaroli, D., Henne, P.D., van Leeuwen, J.F., Süsstrunk, P., Kaltenrieder, P., Adolf, C., Vogel, H., Pasta, S., Anselmetti, F.S., 2016. Vegetation and fire history of coastal north-eastern Sardinia (Italy) under changing Holocene climates and land use. Veg. Hist. Archaeobotany 25, 271–289.

Bernal-Wormull, J.L., Moreno, A., Bartolomé, M., Arriolabengoa, M., Pérez-Mejías, C., Iriarte, E., Osácar, C., Spötl, C., Stoll, H., Cacho, I., Edwards, R.L., 2023. New insights into the climate of northern Iberia during the younger dryas and Holocene: the mendukilo multi-speleothem record. Quat. Sci. Rev. 305, 108006.

Bernardini, P., 2009. Fenici e Punici in Sardegna. In: Atti della XLIV Riunione Scientifica "La Preistoria e la Protostoria della Sardegna", pp. 183–194.

Bini, M., Zanchetta, G., Regattieri, E., Isola, I., Drysdale, R.N., Fabiani, F., Genovesi, S., Hellstrom, J.C., 2020. Hydrological changes during the Roman Climatic Optimum in northern Tuscany (Central Italy) as evidenced by speleothem records and archaeological data. J. Quat. Sci. 35 (6), 791–802.

Blondel, J., 2006. The 'design' of Mediterranean landscapes: a millennial story of humans and ecological systems during the historic period. Hum. Ecol. 34 (5), 713–729.

Boer, W., Nordstad, S., Weber, M., Mertz-Kraus, R., Hönisch, B., Bijma, J., Raitzsch, M., Wilhelms-Dick, D., Foster, G.L., Goring-Harford, H., Nürnberg, D., 2022. New calcium carbonate nano-particulate pressed powder pellet (NFHS-2-NP) for LA-ICP-OES, LA-(MC)-ICP-MS and μXRF. Geostand. Geoanal. Res. 46, 411–432.

Borsato, A., Frisia, S., Fairchild, I.J., Somogyi, A., Susini, A., 2007. Trace element distribution in annual stalagmite laminae mapped by micrometer-resolution X-ray fluorescence: implications for incorporation of environmentally significant species. Geochem. Cosmochim. Acta 71 (6), 1494–1512.

Breitenbach, S.F.M., Rehfeld, K., Goswami, B., Baldini, J., Ridley, H., Kennett, D., Prufer, K., Aquino, V., Asmerom, Y., Polyak, V., 2012. COnstructing proxy-record age models (COPRA). Clim. Past 8 (5), 1765–1779.

Buosi, C., Pittau, P., Paglietti, G., Scanu, G.G., Serra, M., Ucchesu, M., Tanda, G., 2015. A human occupation cave during the Bronze Age: archaeological and palynological applications of a case study in Sardinia (Western Mediterranean). Archaeometry 57 (S1), 212–231.

Burkert, W., 1992. The Orientalizing Revolution: Near Eastern Influence on Greek Culture in the Early Archaic Age. Harvard University Press.

Carmignani, L., Oggiano, G., Barca, S., Conti, P., Salvadori, I., Eltrudis, A., Funedda, A.L., Pasci, S., 2001. Geologia della Sardegna (note illustrative della Carta geologica della Sardegna in scala 1: 200.000). Mem. Descr. Carta Geol. Italia 60, 1–283.

Cheng, H., Lawrence Edwards, R., Shen, C.-C., Polyak, V.J., Asmerom, Y., Woodhead, J., Hellstrom, J., Wang, Y., Kong, X., Spötl, C., Wang, X., Calvin Alexander, E., 2013. Improvements in ^{230}Th dating, ^{230}Th and ^{234}U half-life values, and U–Th isotopic

measurements by multi-collector inductively coupled plasma mass spectrometry. Earth Planet Sci. Lett. 371–372, 82–91.
Cheng, H., Zhang, H., Spötl, C., Baker, J., Sinha, A., Li, H., Bartolomé, M., Moreno, A., Kathayat, G., Zhao, J., Dong, X., Li, Y., Ning, Y., Jia, X., Zong, B., Ait Brahim, Y., Pérez-Mejías, C., Cai, Y., Novello, V.F., Cruz, F.W., Severinghaus, J.P., An, Z., Edwards, R.L., 2020. Timing and structure of the Younger Dryas event and its underlying climate dynamics. Proc. Natl. Acad. Sci. USA 117, 23408–23417.
Cipriani, A., Giovanardi, T., Mazzucchelli, M., Lugli, F., Sforna, M.C., Gualtieri, A.F., Di Giuseppe, D., Gaeta, M., Brunelli, D., 2023. Origin of a carbonate-bearing fluorapatite from tertiary volcanics of the veneto volcanic province. Italy, Miner. Petrolo. 1–22.
Cohen, L., Jarvis, P., Fowler, J., 2013. Practical Statistics for Field Biology. John Wiley & Sons.
Columbu, A., Drysdale, R., Capron, E., Woodhead, J., De Waele, J., Sanna, L., Hellstrom, J., Bajo, P., 2017. Early last glacial intra-interstadial climate variability recorded in a Sardinian speleothem. Quat. Sci. Rev. 169, 391–397.
Columbu, A., Spötl, C., De Waele, J., Yu, T.-L., Shen, C.-C., Gázquez, F., 2019. A long record of MIS 7 and MIS 5 climate and environment from a western Mediterranean speleothem (SW Sardinia, Italy). Quat. Sci. Rev. 220, 230–243.
Columbu, A., Calabrò, L., Chiarini, V., De Waele, J., 2021. Stalagmites: from science application to museumization. Geoheritage 13, 1–11.
Columbu, A., Zhornyak, L.V., Zanchetta, G., Drysdale, R.N., Hellstrom, J.C., Isola, I., Regattieri, E., Fallick, A.E., 2023. A mid-Holocene stalagmite multiproxy record from southern Siberia (Krasnoyarsk, Russia) linked to the Siberian High patterns. Quat. Sci. Rev. 320, 108355.
D'Angeli, I.M., Sanna, L., Calzoni, C., De Waele, J., 2015. Uplifted flank margin caves in telogenetic limestones in the Gulf of Orosei (Central-East Sardinia—Italy) and their palaeogeographic significance. Geomorphology 231, 201–211.
Daeron, M., Drysdale, R.N., Peral, M., Huyghe, D., Blamart, D., Coplen, T.B., Lartaud, F., Zanchetta, G., 2019. Most Earth-surface calcites precipitate out of isotopic equilibrium. Nat. Commun. 10, 429.
De Waele, J., 2009. Evaluating disturbance on Mediterranean karst areas: the example of Sardinia (Italy). Environ. Geol. 58 (2), 239–255.
Delussu, F., 2016. Il riutilizzo dei Nuraghi in età romana nel territorio di Dorgali: layers. Archeologia Territorio Contesti 1, 128–144.
Depalmas, A., 2018. Dal nuraghe a corridoio al nuraghe complesso. In: Il Tempo dei Nuraghi. La Sardegna dal XVIII all'VIII Secolo a. C. Nuoro: Ilisso, pp. 54–60.
Depalmas, A., Melis, R.T., 2011. The Nuragic people: their settlements, economic activities and use of the land, Sardinia, Italy. In: Landscapes and Societies. Springer, pp. 167–186.
di Rita, F., Melis, R.T., 2013. The cultural landscape near the ancient city of Tharros (central West Sardinia): vegetation changes and human impact. J. Archaeol. Sci. 40 (12), 4271–4282.
Dyson, S.L., Rowland, R.J., 2007. Archaeology & History in Sardinia from the Stone Age to the Middle Ages: Shepherds, Sailors, and Conquerors. UPenn Museum of Archaeology, Philadelphia, p. 240.
Drysdale, R., Hellstrom, J.C., Zanchetta, G., Fallick, A.E., Sanchez Goni, M.F., Couchoud, I., McDonald, J., Maas, R., Lohmann, G., Isola, I., 2009. Evidence for obliquity forcing of glacial Termination II. Science 325 (5947), 1527–1531.
Drysdale, R., Couchoud, I., Zanchetta, G., Isola, I., Regattieri, E., Hellstrom, J., Govin, A., Tzedakis, P.C., Ireland, T., Corrick, E., Greig, A., Wong, H., Piccini, L., Holden, P., Woodhead, J., 2020. Magnesium in subaqueous speleothems as a potential palaeotemperature proxy. Nat. Commun. 11 (1), 5027.
Eshel, T., Erel, Y., Yahalom-Mack, N., Tirosh, O., Gilboa, A., 2019. Lead isotopes in silver reveal earliest Phoenician quest for metals in the west Mediterranean. Proc. Natl. Acad. Sci. USA 116 (13), 6007–6012.
Fairchild, I.J., Treble, P.C., 2009. Trace elements in speleothems as recorders of environmental change. Quat. Sci. Rev. 28 (5–6), 449–468.
Faraji, M., Borsato, A., Frisia, S., Hellstrom, J.C., Lorrey, A., Hartland, A., Greig, A., Mattey, D.P., 2021. Accurate dating of stalagmites from low seasonal contrast tropical Pacific climate using Sr 2D maps, fabrics and annual hydrological cycles. Sci. Rep. 11 (1), 1–16.
Faraji, M., Borsato, A., Frisia, S., Mattey, D.P., Drysdale, R.N., Verdon-Kidd, D.C., Malcolm, R., Marca, A., 2022. Controls on rainfall variability in the tropical South Pacific for the last 350 years reconstructed from oxygen isotopes in stalagmites from the Cook Islands. Quat. Sci. Rev. 289, 107633.
Flohr, P., Fleitmann, D., Zorita, E., Sadekov, A., Cheng, H., Bosomworth, M., Edwards, L., Matthews, W., Matthews, R., 2017. Late Holocene droughts in the Fertile Crescent recorded in a speleothem from northern Iraq. Geophys. Res. Lett. 44 (3), 1528–1536.
Frisia, S., Borsato, A., 2010. Karst. Dev. Sedimentol. 61, 269–318.
Frisia, S., 2015. Microstratigraphic logging of calcite fabrics in speleothems as tool for palaeoclimate studies. Int. J. Speleol. 44 (1), 1–16.
Gatti, L., Lugli, F., Sciutto, G., Zangheri, M., Prati, S., Mirasoli, M., Silvestrini, S., Benazzi, S., Tütken, T., Douka, K., Collina, C., 2022. Combining elemental and immunochemical analyses to characterize diagenetic alteration patterns in ancient skeletal remains. Sci. Rep. 12, 5112.
Harper, K., 2017. The Fate of Rome. Climate, Disease and the End of an Empire. Princeton University Press, Princeton and Oxford.
Hendy, C.H., 1971. The isotopic geochemistry of speleothems-I. The calculation of the effects of different modes of formation on the isotopic composition of speleothems and their applicability as palaeoclimatic indicators. Geochem. Cosmochim. Acta 35 (8), 801–824.
Hua, Q., McDonald, J., Redwood, D., Drysdale, R.N., Lee, S., Fallon, S., Hellstrom, J., 2012. Robust chronological reconstruction for young speleothems using radiocarbon. Quat. Geochronol. 14, 67–80.
James, N.P., Jones, B., 2015. Origin of Carbonate Sedimentary Rocks. John Wiley & Sons.
Lechleitner, F., Amirnezhad-Mozhdehi, S., Columbu, A., Comas-Bru, L., Labuhn, I., Pérez-Mejías, C., Rehfeld, K., 2018. The potential of speleothems from western Europe as recorders of regional climate: a critical assessment of the SISAL database. Quaternary 1 (3), 1–31.
Lilliu, G., 1999. La Civiltà Nuragica. Carlo Delfino, Roma, p. 242.
López, P., López Sáez, J.A., Rosario, M., 2005. Studio de la paleovegetación de algunos yacimientos de la Edad del Bronce en el SE de Cerdeña. Anejos de Complutum 10, 91–105.
Magny, M., de Beaulieu, J.L., Drescher-Schneider, R., Vannière, B., Walter-Simonnet, A. V., Miras, Y., Millet, L., Bossuet, G., Peyron, O., Brugiapaglia, E., Leroux, A., 2007. Holocene climate changes in the central Mediterranean as recorded by lake-level fluctuations at Lake Accesa (Tuscany, Italy). Quat. Sci. Rev. 26, 1736–1758.
Malavasi, M., Bazzichetto, M., Bagella, S., Barták, V., Depalmas, A., Gregorini, A., Sperandii, M., Acosta, A., Bagella, S., 2023. Ecology meets archaeology: past, present and future vegetation-derived ecosystems services from the Nuragic Sardinia (1700–580 BCE). People Nat 5 (2), 938–949.
Martín-Chivelet, J., Muñoz-García, M.B., Cruz, J.A., Ortega, A.I., Turrero, M.J., 2017. Speleothem Architectural Analysis: integrated approach for stalagmite-based paleoclimate research. Sediment. Geol. 353, 28–45.
McDermott, F., 2004. Palaeo-climate reconstruction from stable isotope variations in speleothems: a review. Quat. Sci. Rev. 23 (7–8), 901–918.
Muñoz-García, M.B., Cruz, J., Martín-Chivelet, J., Ortega, A.I., Turrero, M.J., López-Elorza, M., 2016. Comparison of speleothem fabrics and microstratigraphic stacking patterns in calcite stalagmites as indicators of paleoenvironmental change. Quat. Int. 407, 74–85.
Orland, I.J., Burstyn, Y., Bar-Matthews, M., Kozdon, R., Ayalon, A., Matthews, A., Valley, J.W., 2014. Seasonal climate signals (1990–2008) in a modern Soreq Cave stalagmite as revealed by high-resolution geochemical analysis. Chem. Geol. 363, 322–333.
Pedrotta, T., Gobet, E., Schwörer, C., Beffa, G., Butz, C., Henne, P.D., Morales-Molino, C., Pasta, S., van Leeuwen, J.F.N., Vogel, H., Zwimpfer, E., Anselmetti, F.S., Grosjean, M., Tinner, W., 2021. 8,000 years of climate, vegetation, fire and land-use dynamics in the thermo-mediterranean vegetation belt of northern Sardinia (Italy). Veg. Hist. Archaeobotany 30, 789–813.
Pittau, P., Buosi, C., Scanu, G.G., 2018. Past environments of Sardinian archaeological sites (Italy, West Mediterranean Sea), based on palynofacies characterization. Acta Palaeobot. 58, 73–93.
Railsback, L.B., Akers, P.D., Wang, L., Holdridge, G.A., Voarintsoa, N.R., 2013. Layer-bounding surfaces in stalagmites as keys to better paleoclimatological histories and chronologies. Int. J. Speleol. 42, 167–180.
Ramos-Román, M.J., Jiménez-Moreno, G., Camuera, J., García-Alix, A., Anderson, R.S., Jiménez-Espejo, F.J., Sachse, D., Toney, J.L., Carrión, J.S., Webster, C., Yanes, Y., 2018. Millennial-scale cyclical environment and climate variability during the Holocene in the western Mediterranean region deduced from a new multi-proxy analysis from the Padul record (Sierra Nevada, Spain). Global Planet. Change 168, 35–53.
Regattieri, E., Zanchetta, G., Isola, I., Zanella, E., Drysdale, R.N., Hellstrom, J.C., Zerboni, A., Dallai, L., Tema, E., Lanci, L., Costa, E., Magrì, F., 2019. Holocene Critical Zone dynamics in an Alpine catchment inferred from a speleothem multiproxy record: disentangling climate and human influences. Sci. Rep. 9 (1), 17829.
Regattieri, E., Zanchetta, G., Drysdale, R.N., Isola, I., Hellstrom, J.C., Dallai, L., 2014. Lateglacial to Holocene trace element record (Ba, Mg, Sr) from Corchia cave (apuan alps, central Italy): paleoenvironmental implications. J. Quat. Sci. 29 (4), 381–392.
Regattieri, E., Zanchetta, G., Drysdale, R.N., Isola, I., Woodhead, J.D., Hellstrom, J.C., Giaccio, B., Greig, A., Baneschi, I., Dotsika, E., 2016. Environmental variability between the penultimate deglaciation and the mid Eemian: insights from Tana che Urla (central Italy) speleothem trace element record. Quat. Sci. Rev. 152, 80–92.
Ridley, H.E., Asmerom, Y., Baldini, J.U., Breitenbach, S.F., Aquino, V.V., Prufer, K.M., Culleton, B.J., Polyak, V., Lechleitner, F.A., Kennett, D.J., 2015. Aerosol forcing of the position of the intertropical convergence zone since AD 1550. Nat. Geosci. 8 (3), 195.
Sabato, D., Peña-Chocarro, L., Ucchesu, M., Sarigu, M., Del Vais, C., Sanna, I., Bacchetta, G., 2019. New insights about economic plants during the 6th-2nd centuries BC in Sardinia, Italy. Veg. Hist. Archaeobotany 28, 9–16.
Sadori, L., Jahns, S., Peyron, O., 2011. Mid-Holocene vegetation history of the central Mediterranean. Holocene 21, 117–129.
Stephens, L., Fuller, D., Boivin, N., Rick, T., Gauthier, N., Kay, A., Marwick, B., Armstrong, C.G., Barton, C.M., Denham, T., Douglass, K., 2019. Archaeological assessment reveals Earth's early transformation through land use. Science 365, 897–902.
Surić, M., Columbu, A., Lončarić, R., Bajo, P., Bočić, N., Lončar, N., Drysdale, R., Hellstrom, J., 2021. Holocene hydroclimate changes in continental Croatia recorded in speleothem $\delta^{13}C$ and $\delta^{18}O$ from Nova Grgosova Cave. Holocene 31 (9), 1401–1416.
Treble, P.C., Baker, A., Abram, N.J., Hellstrom, J.C., Crawford, J., Gagan, M.K., Borsato, A., Griffiths, A., Bajo, P., Markowska, M., Priestley, S., Hankin, S., Paterson, D., 2022. Ubiquitous karst hydrological control on speleothem oxygen isotope variability in a global study. Commun. Earth Environ. 3 (1), 29.
Ucchesu, M., Pena-Chocarro, L., Sabato, D., Tanda, G., 2015. Bronze Age subsistence in Sardinia, Italy: cultivated plants and wild resources. Veg. Hist. Archaeobotany 24, 343–355.

Ucchesu, M., Sarigu, M., Del Vais, C., Sanna, I., Guy, D., Grillo, O., Bacchetta, G., 2017. First finds of *Prunus domestica* L. in Italy from the Phoenician and Punic periods (6th-2nd centuries BC). Veg. Hist. Archaeobotany 26, 539–549.

Vanghi, V., Borsato, A., Frisia, S., Drysdale, R., Hellstrom, J., Bajo, P., 2018. Climate variability on the Adriatic seaboard during the last glacial inception and MIS 5c from Frasassi Cave stalagmite record. Quat. Sci. Rev. 201, 349–361.

Voarintsoa, N.R.G., Railsback, L.B., Brook, G.A., Wang, L., Kathayat, G., Cheng, H., Li, X., Edwards, R.L., Rakotondrazafy, A.F.M., Madison Razanatseheno, M.O., 2017. Three distinct Holocene intervals of stalagmite deposition and nondeposition revealed in NW Madagascar, and their paleoclimate implications. Clim. Past 13 (12), 1771–1790.

Weber, M., Lugli, F., Jochum, K.P., Cipriani, A., Scholz, D., 2018. Calcium carbonate and phosphate reference materials for monitoring bulk and microanalytical determination of Sr isotopes. Geostand. Geoanal. Res. 42 (1), 77–89.

Zanchetta, G., Regattieri, E., Isola, I., Drysdale, R.N., Baneschi, I., Hellstrom, J.C., 2016. The so-called "4.2 event" in the central Mediterranean and its climatic teleconnections. Alpine and Mediterranean Quaternary 29 (1), 5–17.

Zanchetta, G., Baneschi, I., Magny, M., Sadori, L., Termine, R., Bini, M., Vannière, B., Desmet, M., Natali, S., Luppichini, M., Pasquetti, F., 2022. Insight into summer drought in southern Italy: palaeohydrological evolution of Lake Pergusa (Sicily) in the last 6700 years. J. Quat. Sci. 37, 1280–1293.